A STUDY OF THE OPTICAL ABSORPTION AND PHOTOCONDUCTIVITY
OF GAMMA-IRRADIATED LiF

by

MILTON HENRY RICHTER

B.S., Valparaiso University, 1974

A MASTER'S THESIS

submitted in partial fulfillment of the
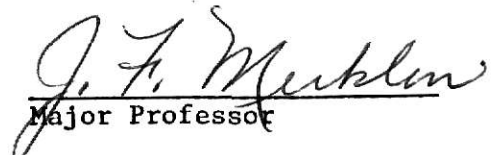requirements for the degree

MASTER OF SCIENCE

Department of Nuclear Engineering

Kansas State University

Manhattan, Kansas

1976

Approved by:

J. F. Merklin
Major Professor

TABLE OF CONTENTS

LIST OF TABLES

I. Introduction

The passage of ionizing radiation through an alkali halide produces a coloring of the crystal[1,2]. The production of color results from the trapping of holes and electrons, produced by radiation, at crystal imperfections and impurity sites. The defect centers formed by the trapped charges are called "color centers", and they have excited states which allow absorption of photons normally transmitted by the crystal[3,4]. The F-center is the principal color center produced by ionizing radiation[5,6].

At room temperature, LiF is a highly insulating solid and is optically transparent in the visible and ultraviolet region of the spectrum[7,8]. In the band picture of solids, LiF is described by a filled valence band and an empty conduction band with a forbidden energy gap of about 13.5 eV[9]. The ground and excited states of the F-center are localized energy levels in the forbidden energy gap of the crystal. The transition from the ground state to the first excited state on absorption of light gives rise to the F-center's optical absorption band. The maximum of the F-center absorption band in LiF is at 250 nm at room temperature[4,6,7]. There are other color centers, produced by radiation, which demonstrate similar behavior as the F-center. Thus, several absorption bands can be observed in an optical absorption measurement in the visible and ultraviolet region of the spectrum[4,5,6,7].

It has been shown that illumination of alkali halides containing F-centers with light in the F-center band causes photoconductivity[10,11,12]. Nelson observed room temperature photoconductivity in LiF in the spectral range from 400 nm to 200 nm[13]. Further, some alkali halides exhibit photoconductivity by electrons and holes from other defect centers and impurities[6,7,14,15,16,17].

A recent study was done by Marrs on the optical absorption and photo-conductivity of irradiated LiF. Marrs observed a small absorption band, which he labeled the Y-center absorption band, that appeared as a shoulder on the long-wavelength side of the F-center absorption band. Photoconductivity measurements indicated a photocurrent peak at approximately the same energy as that of the Y-center absorption band. Marrs proposed that the Y-center was an interstitial positive ion impurity adjacent to an F-center[18].

The objective of this research is to study the photoconductivity of LiF, obtained from Harshaw Chemical Corporation and Optovac Chemical Corporation, in the temperature range of 85 °K to 300 °K and to study the optical absorption of the Y-center at 90 °K and 300 °K. The LiF, obtained from the two suppliers, have different impurity concentrations which could possibly identify the positive ion impurity believed to be causing the Y-center.

II. Theory

2.1 Defect Centers

The exposure of alkali halides to ionizing radiation promotes electrons from the valence band to the conduction band. The electrons and holes can be trapped at crystal imperfections and impurity sites causing color centers[5,6]. Every color center has localized energy levels in the forbidden energy gap of the crystal. The transition of the electron from the ground state to an excited state upon the absorption of a photon gives rise to an absorption band characteristic of the color center[4,6]. The F-center is the dominant color center produced in alkali halides and is formed when an electron is trapped at a halogen ion vacancy (negative ion vacancy)[19].

When alkali halides are subjected to prolonged irradiation, aggregates of the F-center are formed. Two F-centers as nearest neighbors constitute an M-center, and three adjacent F-centers an R-center[4,19]. At temperatures above room temperature the M and R-centers are unstable, and they can be decomposed by annealing at 100 °C[4]. Annealing reduces the strength of an absorption band by irreversibly destroying the site in the lattice which can absorb a photon. Annealing is not to be confused with bleaching; in bleaching the strength of the absorption band is reduced by depopulation of the ground state of the defect[19].

F-centers in the alkali halides exhibit characteristic absorption bands that are fairly broad at room temperature. With decreasing temperature, the bands narrow and shift toward shorter wavelengths. The temperature dependence of the F-center absorption bands can be qualitatively explained in terms of a model in which the trapped electron is treated as a particle-in-a-box[6,20,21]. The

difference in energy between the ground state and the first excited state for a particle-in-a-box is given by[6,20]

$$E_2 - E_1 = \frac{3\pi^2 h^2}{8ma^2} , \qquad (1)$$

where

E_2 = energy of first excited state,

E_1 = energy of ground state,

m = mass of the free electron = 9.1091 x 10^{-31} kg,

h = Planck's constant divided by 2π = 1.054 x 10^{-34} J·s,

a = nearest neighbor distance = 0.2013 nm.

As the temperature decreases, the nearest neighbor distance, a, decreases due to contraction of the lattice. This decrease causes an increase in the difference in energy between the ground and excited state. The width of the band arises from the interaction of the F-center with the vibration of the neighboring ions about their zero-point position[20,21]. As the temperature decreases the average amplitude of the thermal vibrations of the ions will also decrease, thus causing a reduction in the variation of the dimensions of the box. Qualitatively it is seen that a reduction in the variation of the dimensions of the box will result in the narrowing of the width of the absorption band[20,21].

2.2 Processes in a Photoconductor

A photoconductor in the broadest sense is defined as any material whose electrical·conductivity can be increased by the absorption of photons[22,23]. The absorption of photons in a semiconductor or insulator is a quantum process in which electrons are raised from trapping sites or the valence band to the conduction band[5,22]. For the case of removing an electron from the valence band, a free positive hole is also produced. If a voltage is applied to the

crystal, the free electrons and free holes should drift in opposite directions, contributing to an electric current[5].

Some of the electronic transitions commonly found in photoconductors are shown in Figs. 1, 2, and 3[10]. These transitions can be divided into three types: 1) absorption and excitation, 2) trapping and capture, and 3) recombination.

Figure 1 illustrates the four possible types of absorption and excitation transitions that result in photoconductivity. Transition 1 corresponds to absorption by the atoms of the crystal itself, producing a free electron and a free hole for each photon absorbed. Transition 2a corresponds to absorption at localized imperfections in the crystal, producing a free electron and a hole bound in the neighborhood of the imperfection for each photon absorbed. Transition 2b is very similar to 2a, the only difference being that the electron is promoted to an excited state below the conduction band yet close enough to be thermally promoted into the band. Transition 3 corresponds to absorption, raising an electron from the valence band to an unoccupied imperfection level, producing a free hole and an electron bound in the neighborhood of the imperfection for each photon absorbed.

Once electrons and holes have been freed by absorption of a photon of sufficient energy, they will remain free until they are captured at an imperfection. The capturing centers can be classified in two groups:[17] 1) trapping centers - if the captured carrier has a greater probability of being thermally re-excited to the conduction band than of recombining with a carrier of opposite sign at the imperfection; 2) recombination centers - if the captured carrier has a greater probability of recombining with a carrier of opposite sign at the imperfection than of being re-excited to the conduction band. Figure 2 shows trapping and thermal release of electrons in electron traps (transitions 5 and

THIS BOOK
CONTAINS
NUMEROUS PAGES
WITH DIAGRAMS
THAT ARE CROOKED
COMPARED TO THE
REST OF THE
INFORMATION ON
THE PAGE.

THIS IS AS
RECEIVED FROM
CUSTOMER.
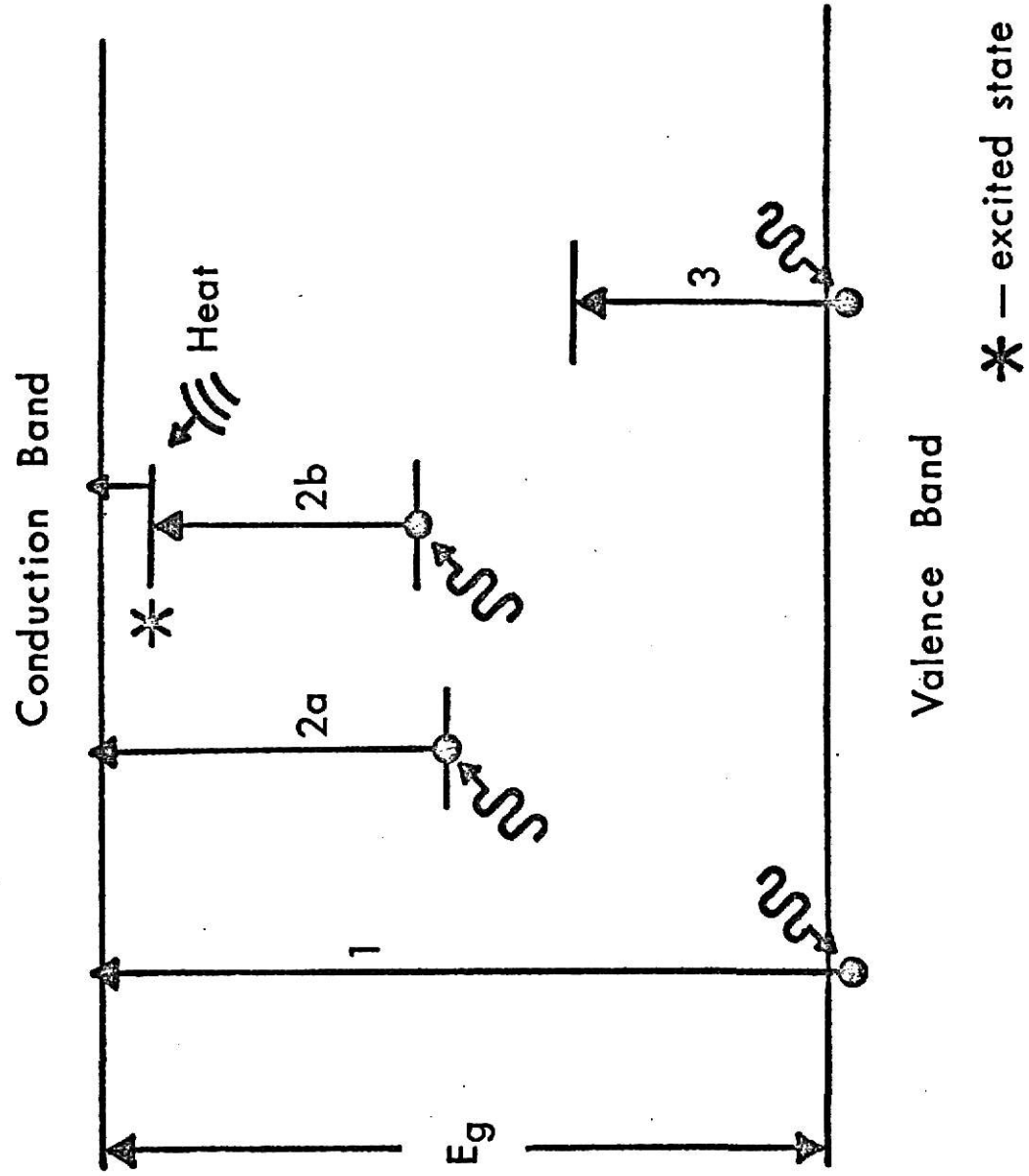
FIGURE 1: Absorption and excitation processes in a photoconductor
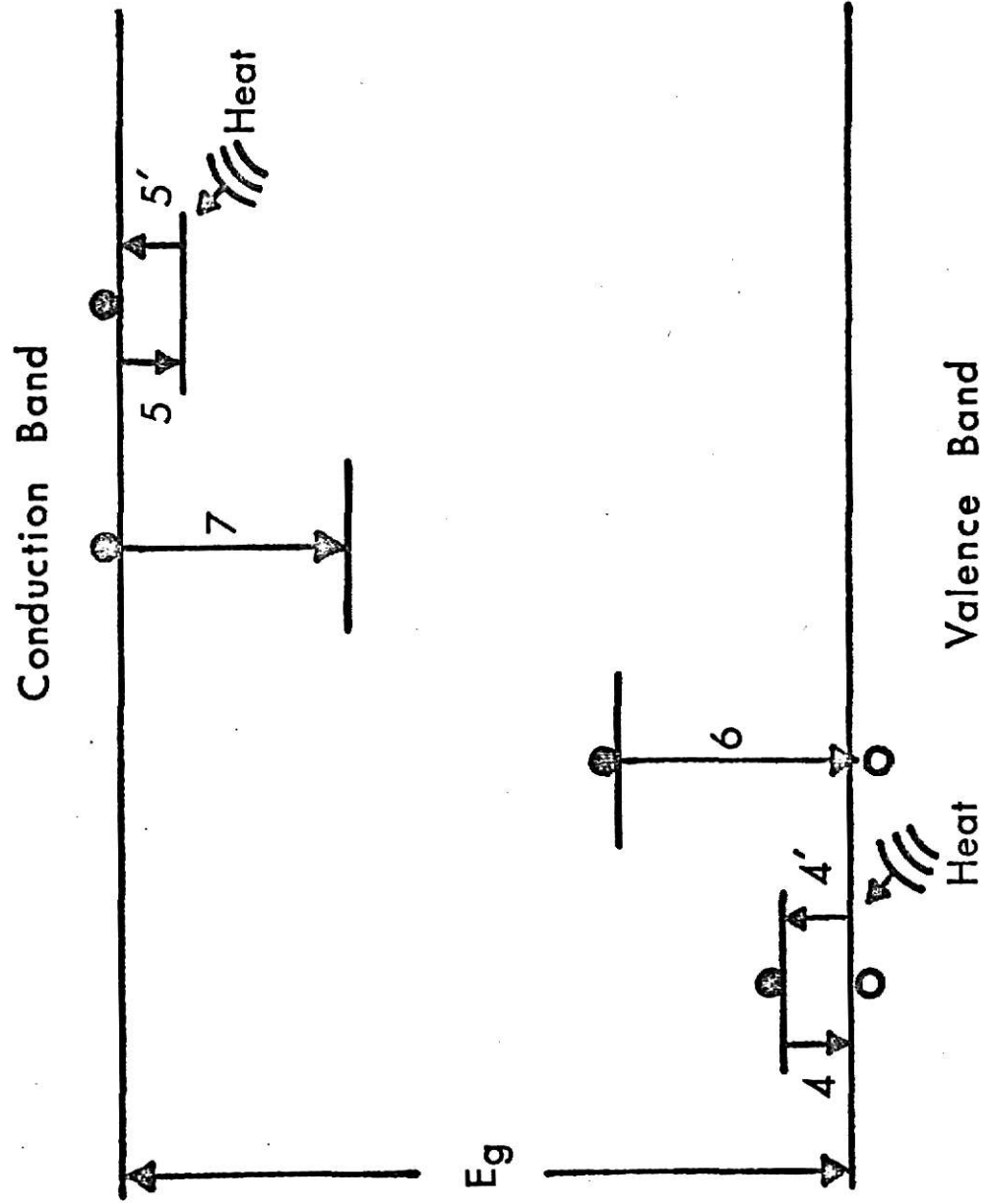
FIGURE 2: Trapping and capture processes in a photoconductor

5'), and trapping and thermal release of holes in hole traps (electron transitions 4 and 4'). The capture of an electron in a recombination center is shown by transition 7. The capture of a hole in a recombination center by an electron transition is shown by transition 6.

Three types of recombination transitions are shown in Fig. 3. The free electron may combine directly with a free hole, depicted by transition 8. Transition 9 illustrates the capture of a free electron at an excited recombination center containing a hole and transition 10 illustrates a free hole being captured at an excited recombination center containing an electron.

2.3 Characteristic Relations of Photoconductivity

The conductivity of an insulator or semiconductor is expressed as:

$$\sigma = e(n\mu_n + p\mu_p) , \qquad (2)$$

where σ is the conductivity, e is the charge of the carrier, n and p are the densities of free electrons and holes, respectively, and μ_n and μ_p are the electron and hole mobilities. In many discussions of photoconductivity a simplifying assumption is made; the photoconductivity is dominated by one of the carriers so that the contribution of the other can be effectively neglected. Equation (2) becomes

$$\sigma = ne\mu , \qquad (3)$$

and is applicable to either free electrons or free holes.

Since e in Eq. (3) is a constant, a change in conductivity (σ) can only result from a change in the density of free charge carriers (n), or from a change in the mobility of the charge carriers (μ), as shown in

$$\Delta\sigma = e\mu\Delta n + en\Delta\mu . \qquad (4)$$

9
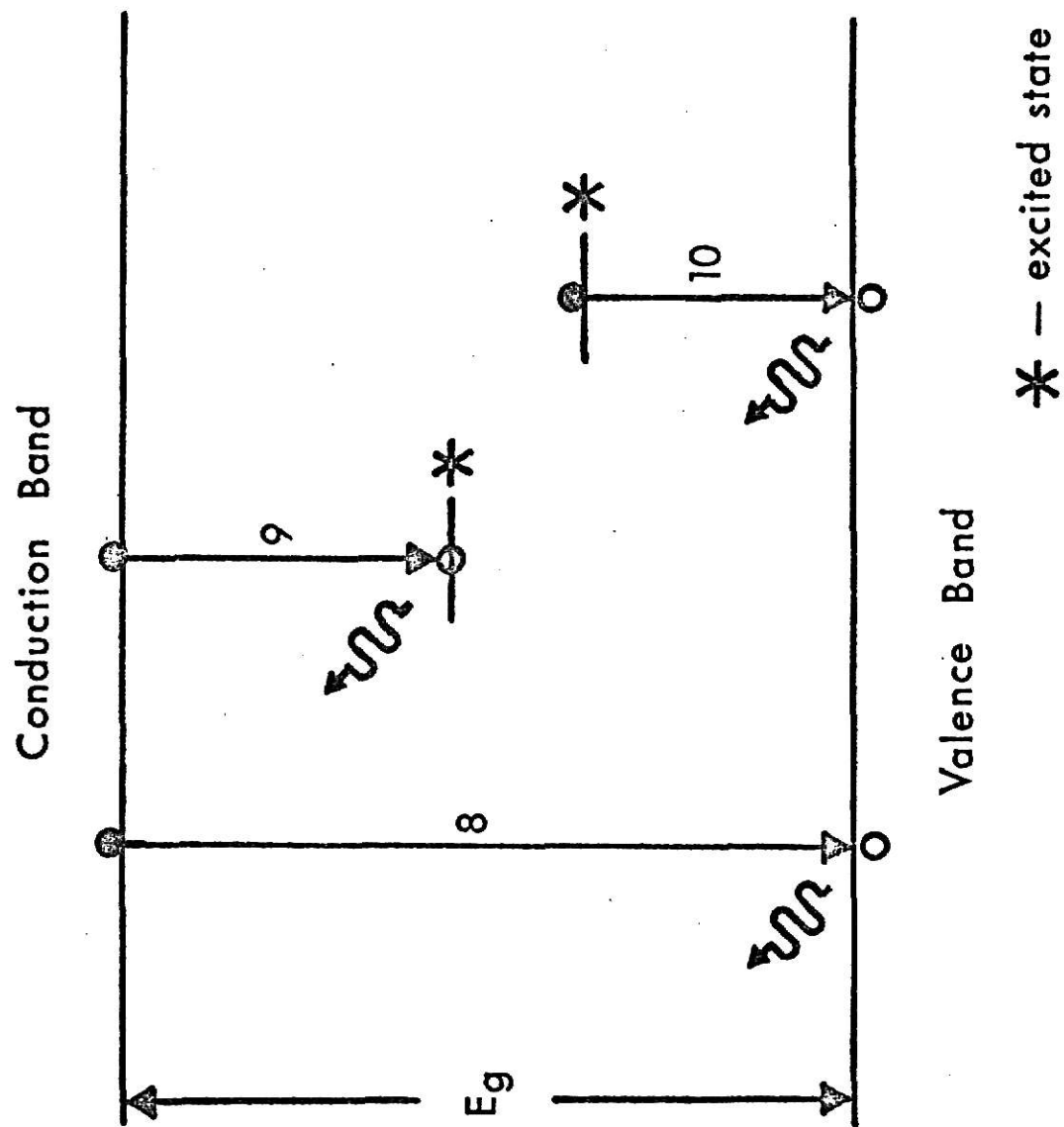
FIGURE 3: Recombination processes in a photoconductor

The density of free charge carriers (n) in steady state is given by:

$$n = f\tau , \qquad\qquad (5)$$

where f is the number of charge carriers freed per unit volume per unit time and τ is the free lifetime of the charge carrier. The free lifetime is the time that the charge carrier is free to contribute to the conductivity.

The change in the density of free charge carriers, Δn, can be related to a change in the excitation density, Δf, and also to a change in the lifetime of the free charge carriers, $\Delta \tau$. Using Eq. (5), Δn can be written as

$$\Delta n = \tau \Delta f + f \Delta \tau . \qquad\qquad (6)$$

Equation (4) can be rewritten as

$$\Delta \sigma = e\mu\tau\Delta f + e\mu f \Delta \tau + en\Delta \mu . \qquad\qquad (7)$$

The first term in Eq. (7), $e\mu\tau\Delta f$, represents the conductivity change due to a change in the density of photoexcitation. It has been observed that the quantum efficiency for the production of free charge carriers in alkali halides varies slowly with decreasing temperature until a temperature characteristic of the particular alkali halide is reached. Below this temperature, which is not known in LiF, the quantum efficiency decreases rapidly[4,7,16]. A decrease in temperature would result in a change in the density of free charge carriers because f is directly proportional to the quantum efficiency.

The second term, $e\mu f \Delta \tau$, represents the conductivity change due to a change in the lifetime of the free charge carriers, $\Delta \tau$. A change in the mean lifetime results when a change occurs in the relative importance of the various mechanisms which govern the rates of charge carrier removal from and emission into the conduction band. Examples are; a change in the density of the free charge carriers, and the filling of trapping levels and recombination centers[10,19,23].

The third term of Eq. (7), $en\Delta \mu$, represents the conductivity change due to a change in the mobility of the free charge carrier. Some causes for mobility change are:

1) A material may be nonhomogeneous, where the number of free holes and free electrons are not uniform throughout the material, in such a way that the passage of current may be impeded by potential barriers within the material. Photoexcitation may lead to a reduction in the height of these barriers and thus increase the conductivity of the material[10].

2) Change in crystal temperature will change the mobility[4,24]. At high temperature, scattering by optical phonons limits the mobility. As the temperature decreases the mobility is limited by the crystal purity[24].

III. Experimental Procedure

Optical absorption spectra and photoconductivity excitation spectra of LiF were measured in the spectral range of 700 nm to 200 nm and 370 nm to 200 nm, respectively, with unpolarized light and light polarized in the [011] and [0$\bar{1}$1] directions relative to the crystal axis. For all measurements, the incident light was normal to the [100] face of the crystal (see Fig. 4).

3.1 Experimental Samples

The LiF crystals were obtained from the Harshaw Chemical Corporation and Optovac Chemical Corporation in 1975. The original dimensions of the crystals received were 1.0 x 1.0 x 1.0 cm and 1.0 x 1.0 x 0.1 cm. The 1.0 x 1.0 x 1.0 cm crystals were cleaved to obtain optical absorption samples of dimensions 1.0 x 1.0 x 0.5 cm. The 1.0 x 1.0 x 0.1 cm crystals were cleaved to obtain photoconductivity excitation samples of dimensions 0.5 x 0.5 x 0.1 cm.

A quantitative Neutron Activation Analysis was run on the Harshaw and Optovac crystals used in this work, and Harshaw crystals obtained in 1972 used in a previous work[18], to determine the impurity concentrations. The Harshaw crystals (1975) contained aluminum, at a concentration of 2.5 $\pm$ 0.8 parts per million (ppm). Aluminum and magnesium were found in the Optovac crystals, at concentrations of 3.5 $\pm$ 0.8 ppm and 32.0 $\pm$ 8.0 ppm, respectively. The 1972 Harshaw crystals contained aluminum at a concentration of 22.5 $\pm$ 1.0 ppm and magnesium at 51.0 $\pm$ 11.0 ppm. The specifics of the Neutron Activation Analysis are given in Appendix A.

Two other differences exist between the Harshaw and Optovac crystals:

1) The Harshaw crystals were cleaved and polished, whereas, the Optovac crystals were cut by a diamond saw.
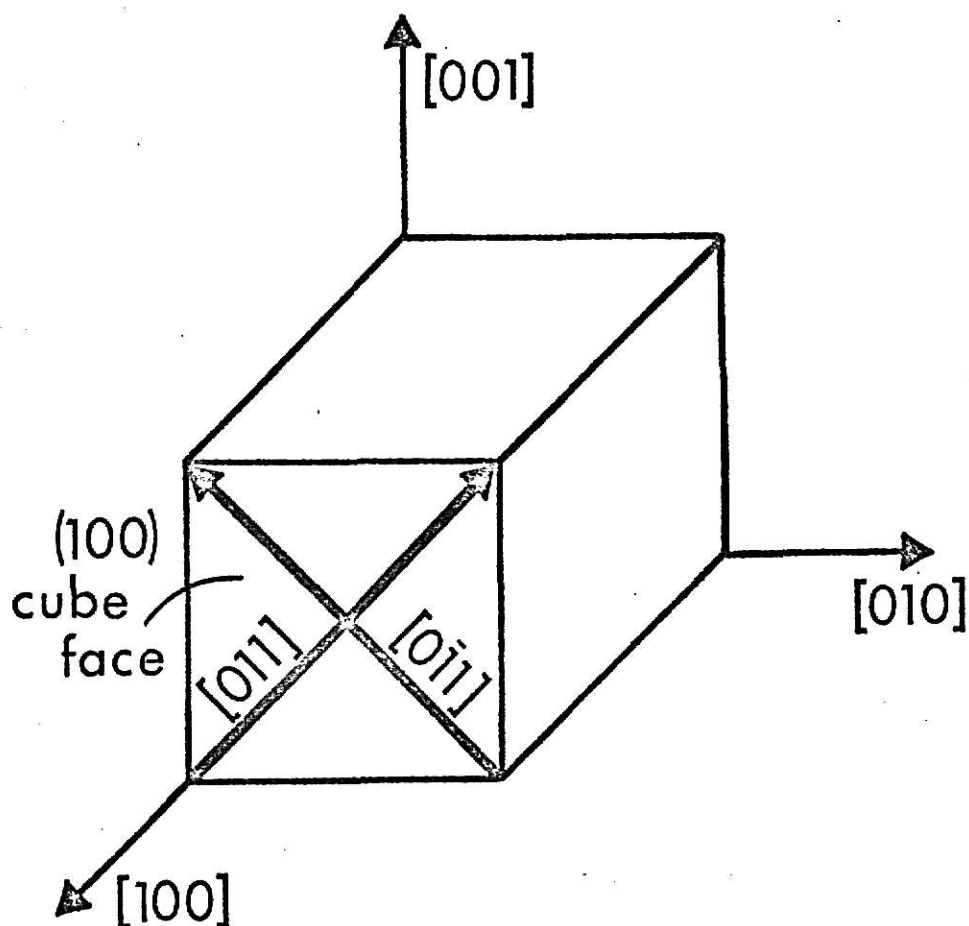
FIGURE 4: Crystallographic representation of the direction of
propagation and the direction of the polarization of
the incident light. Dark arrows denote the polarization
of the incident light relative to the crystal axis.
The incident beam of light was normal to the [100]
face of the crystal.

2) Harshaw Chemical Corporation stated that their crystals had been previously irradiated[25], whereas, the past radiation history of the Optovac crystals is unknown.

3.2 Thermal Annealing

Prior to gamma irradiation all samples were annealed at 450 °C for 24 hours to provide a uniform distribution of vacancies throughout the samples. They were then quick quenched to room temperature in air. The purpose of the quick quenching was to freeze in vacancies formed during the high temperature anneal.

Post-irradiation thermal annealing was also done. The irradiated samples were annealed at 100 °C for 30 minutes and again quick quenched to room temperature. This anneal destroys the larger F-center aggregates so as to eliminate any possible interactions between these centers and centers of interest.

3.3 Gamma Irradiation

The LiF samples were irradiated in the irradiation chamber of the Gamma-cell (AECL 220). The Gammacell was loaded on March 15, 1965 with a 3,963 curie ^{60}Co source.

The sample was placed on a polyethylene disk which fits inside the irradiation chamber of the Gammacell. The polyethylene disk was fabricated by Kaiseruddin in an earlier work[26]. Kaiseruddin determined the position in the irradiation chamber at which the samples would receive the same dose as if they had been positioned in the geometrical center of the chamber. The disk positioned the sample 2-3/4 inches above the base of the chamber and 2 inches from the center axis of the chamber[26]. The dose rate at this position was 21.9

rad/sec, as of January 18, 1976. The desired exposure time can be preset on the Gammacell timer which is activated when the irradiation chamber is in position. The chamber is raised automatically when the sample has been irradiated for the preset time.

3.4 Optical Absorption Measurements

Optical absorption spectra were made using a Cary-14 Spectrophotometer. The spectra were measured with polarized and unpolarized light at temperatures of 90 °K and 300 °K. Measurements were made before and after irradiation of the samples. The spectra of the unirradiated samples were used as background, and were subtracted from the spectra of the irradiated crystals to show the effects of gamma irradiation.

A schematic of the dewar used in the absorbance measurements is shown in Fig. 5. The sample was in vacuum, and was held on the copper cold-finger by Eccotherm TC-4 conducting grease (Emerson and Cuming Inc., Canton, Mass.) which gave good thermal contact.

For optical absorption spectra measured with polarized light, a linear polarizer (Polacoat Inc.) with a spectral range of 240 nm to 400 nm was used.

3.5 Optical Bleaching

Optical absorption samples were bleached with either unpolarized light or light polarized in the [011] and [0$\bar{1}$1] direction. The wavelength of the bleaching light was 254 nm or 280 nm at 300 °K, and 244 nm or 280 nm at 90 °K.

The equipment arrangement that was used to optically bleach the samples is shown in Fig. 6. Monochromatic light for optical bleaching was obtained from the combination of a 100 watt Mercury Arc Lamp (Bausch and Lomb, Model
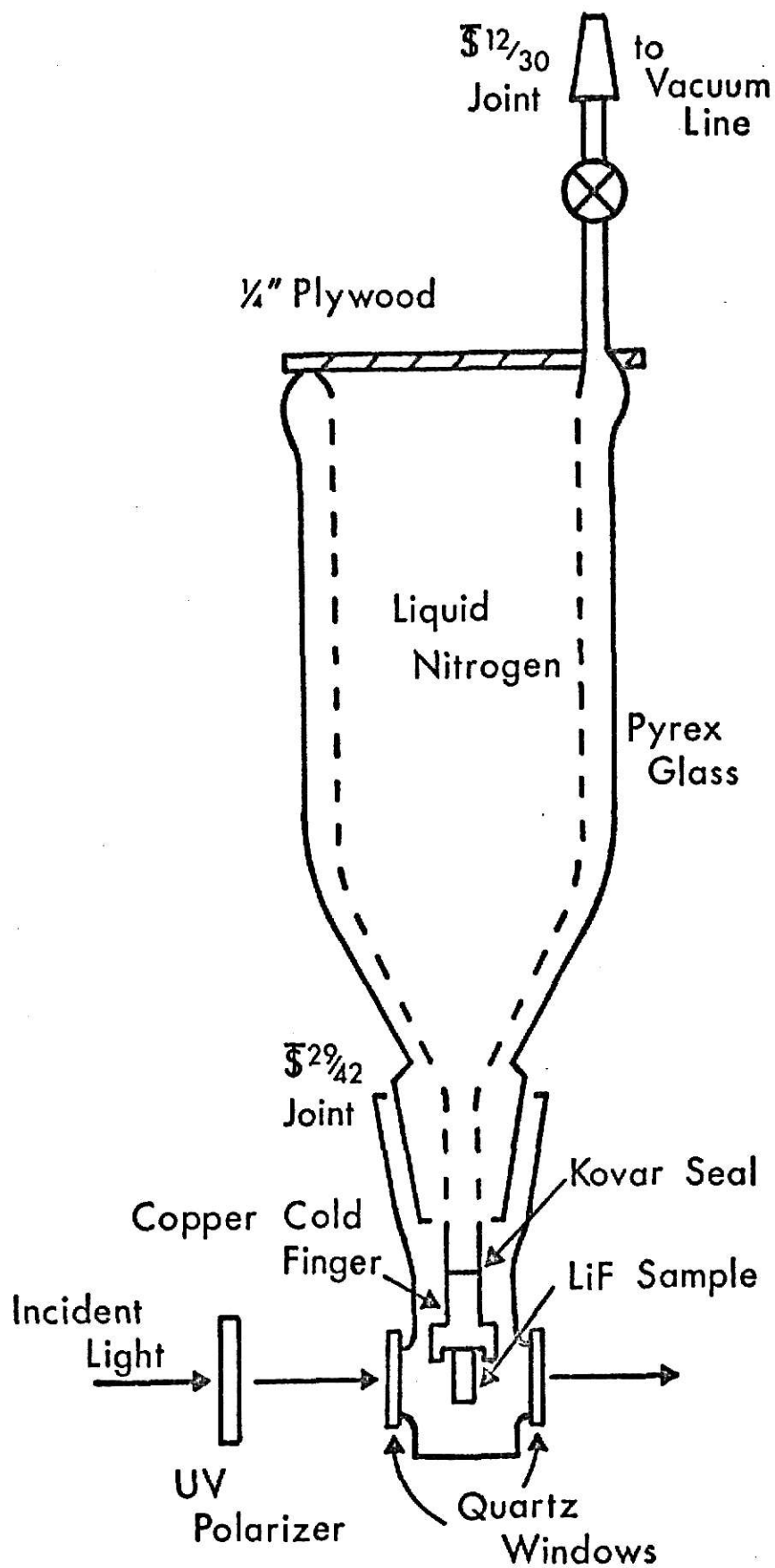
FIGURE 5: Glass dewar sample holder for optical absorption measurements
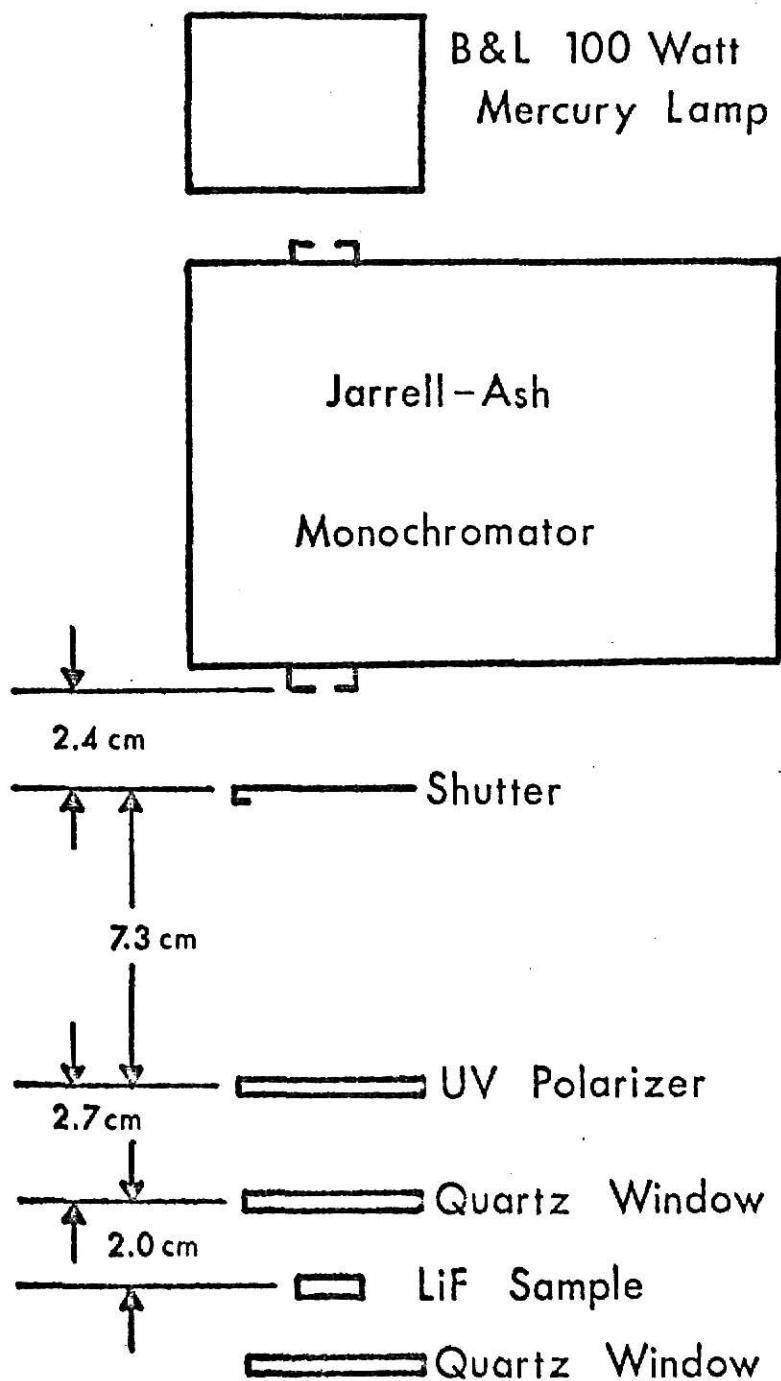
FIGURE 6: Experimental arrangement used in determining the effect of optical bleaching on the optical absorption spectra

HP-100) and a Jarrell-Ash .25 meter Ebert Monochromator (Model 82-410). The monochromator has a one millimeter exit slit which gives a bandpass of 1.6 nm.

. For optical bleaching with polarized light, the Polacoat linear polarizer was placed between the monochromator and sample.

3.6 Photoconductivity Measurements

The photoconductivity excitation spectra were measured with polarized and unpolarized light at the following temperatures; 85 °K, 128 °K, 171 °K, 214 °K, 257 °K, and 300 °K. The light was polarized in the [011] and [0$\bar{1}$1] directions.

Photoconductivity spectra were made using a Cary-401 Vibrating Reed Electrometer. The electrometer was used to measure the change in conductivity of the sample due to photoexcitation. The Cary-401 measured the change in the voltage drop across its input resistor.

The experimental arrangement that was used to obtain the photoconductivity spectra is shown in Figs. 7, 8, and 9. The light source was composed of a LPS 251 Lamp Power Supply, LH 150 Lamp Housing, and a 150 watt Xenon Lamp, made by Schoeffel Instrument Corporation. The LH 150 Lamp Housing was provided with a focusing lens and shutter.

Monochromatic light for photoexcitation of the samples was obtained from the combination of the light source and a Bausch and Lomb Grating Monochromator (Model 33-88-01). The monochromator has entrance and exit slits of 2.68 nm and 1.5 nm respectively, providing a bandpass for the monochromator of 5 nm.

The vacuum chamber, which contained the sample, was mounted on the monochromator. A quartz window on one end of the vacuum chamber allowed the light from the monochromator to enter the vacuum chamber and strike the surface of the sample. The sample holder was positioned on a copper cold-
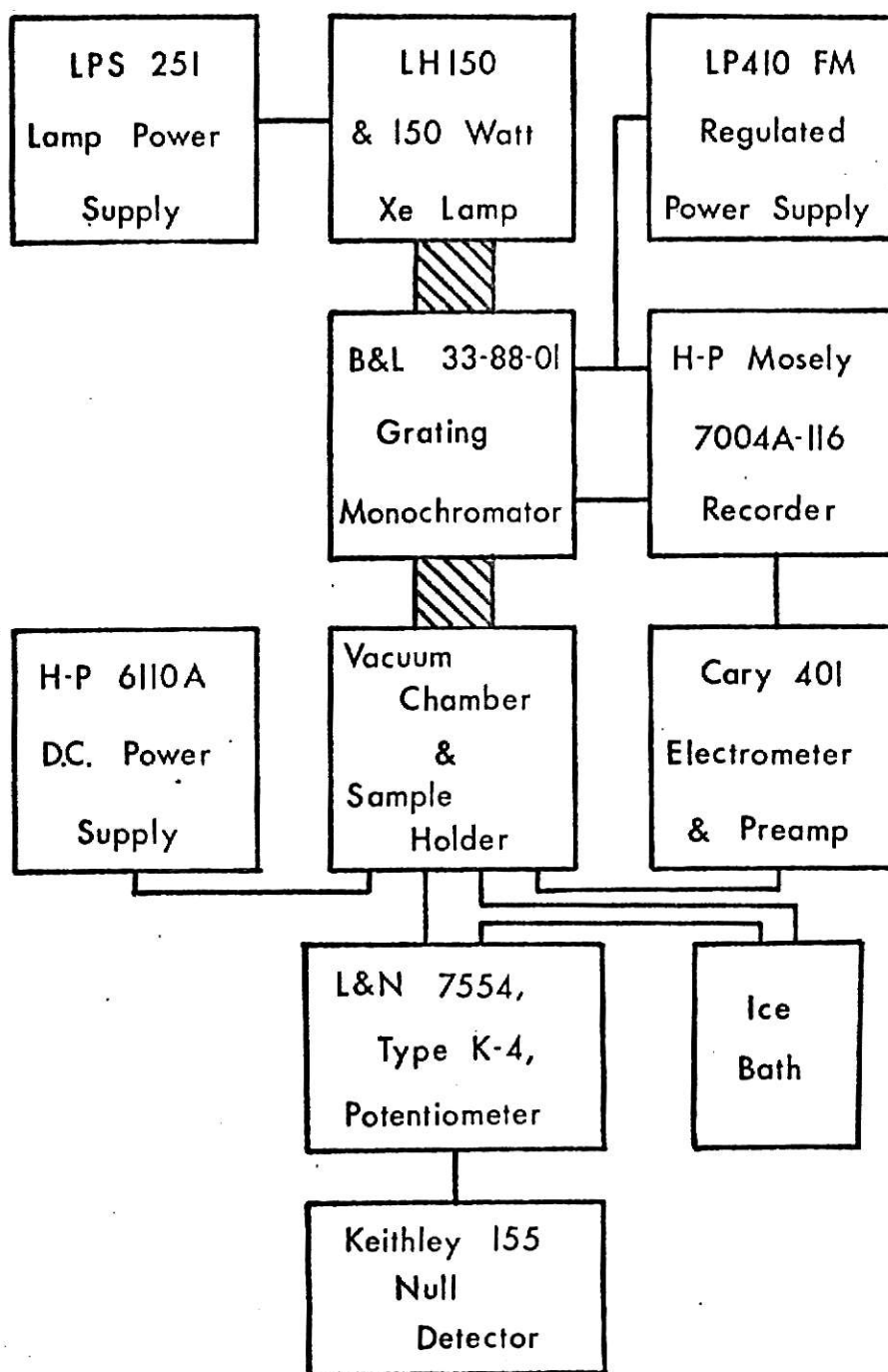
FIGURE 7: Block diagram of the experimental equipment used for the photoconductivity measurements
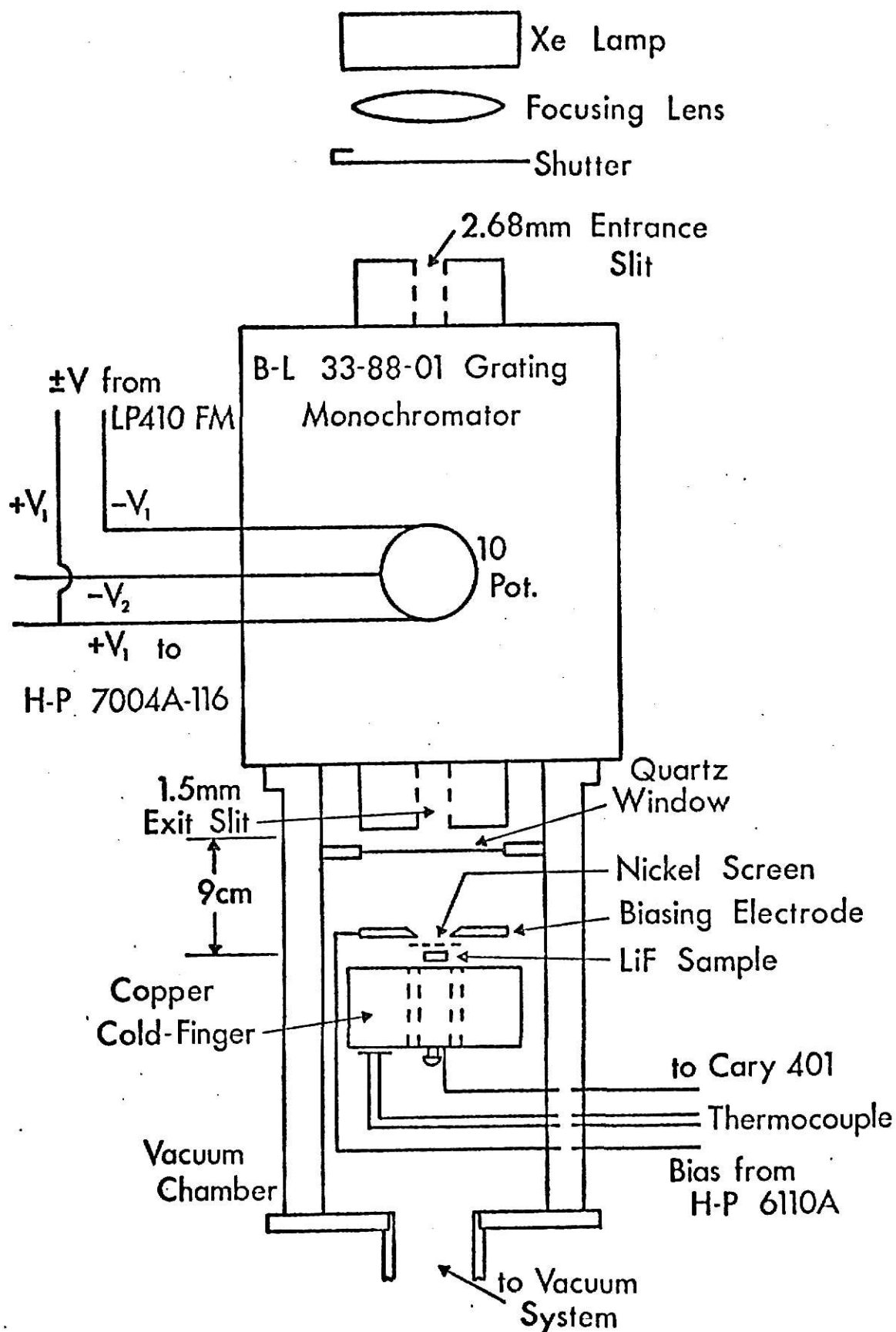
FIGURE 8: Top-view of the Bausch and Lomb monochromator and vacuum chamber used in the photoconductivity measurements
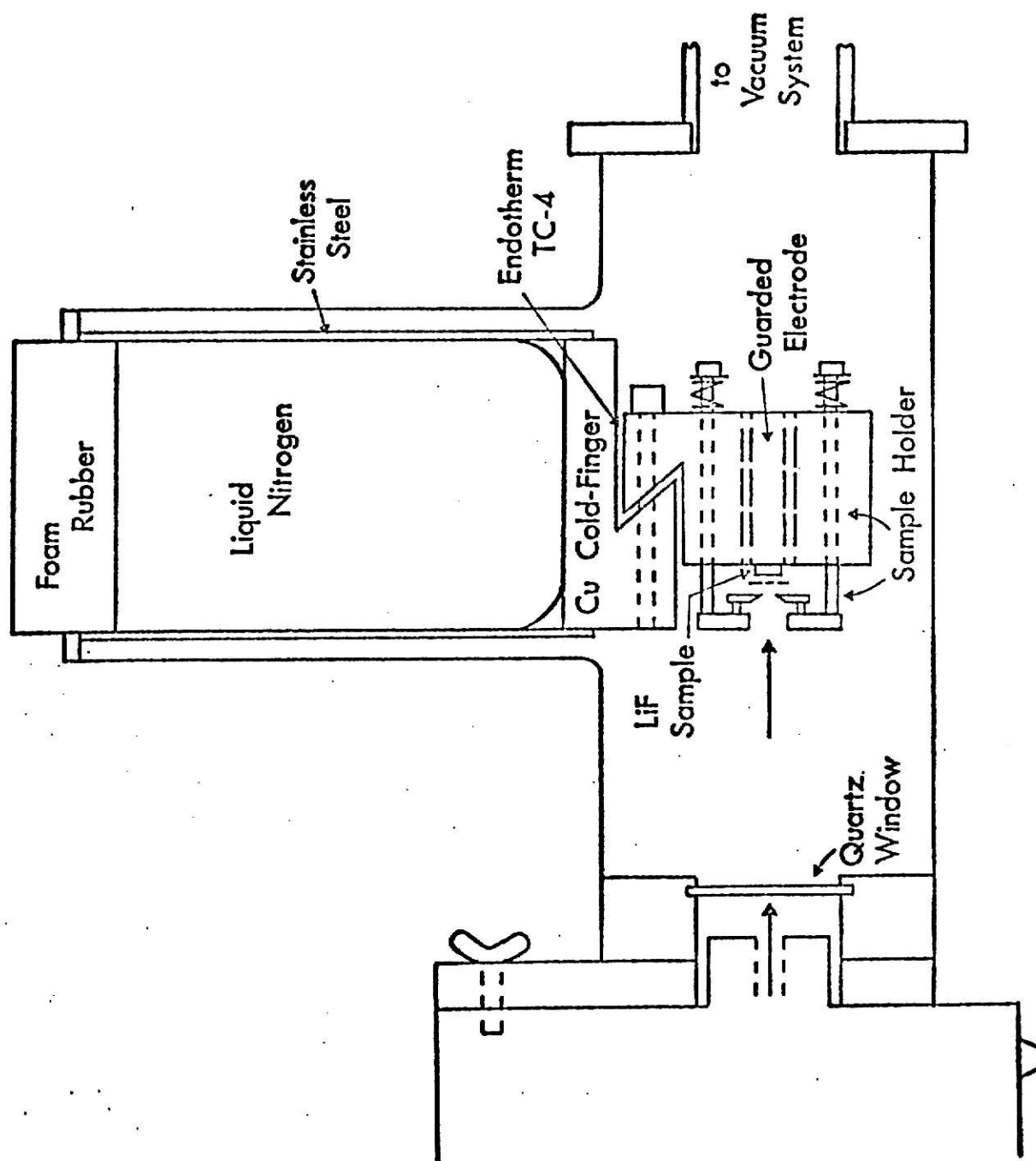
FIGURE 9: Side-view of the vacuum chamber, cold-finger, and sample holder used in the photoconductivity measurements

finger in the vacuum chamber. Eccotherm TC-4 conducting grease was applied to the area between the cold-finger and sample holder.

Since spectra at various temperatures had to be obtained, a copper-constantan thermocouple was attached to the copper sample holder with General Electric Adhesive Varnish, No. 7031. The reference junction of the thermocouple was held at 0 °C in an ice bath and the thermocouple's e.m.f. was measured with a Leeds and Northrup Potentiometer (Model 7554, Type K-4), and a Keithley Null Detector Microvoltmeter (Model 155).

The biasing of the sample was done with a Hewlett-Packard D.C. Power Supply (Model 6110A). A bias voltage of -1000 volts was applied to the front electrode. The biasing electrode was outfitted with a 0.126 cm^2 hole to illuminate the sample. A nickel screen, mesh size 70 squares per inch, was placed between the sample and the biasing electrode to insure uniformity of the electric field. The absorbance of the nickel screen was 0.05 absorbance units.

The input to the electrometer was attached to the rear electrode. The rear electrode was guarded electrically, by a guard ring, to protect the electrometer input against leakage currents.

The photoconductivity spectra were recorded on a Hewlett-Packard X-Y Plotter (Model 7004A-116). The output of the electrometer was recorded on the Y-axis as a function of incident photon wavelength, which was recorded on the X-axis. To scan from 370 nm to 200 nm, a wavelength drive was connected to the wavelength control of the monochromator. The wavelength drive consisted of an A.C. synchronous motor and gear reduction, a 10,000 ohm, 3/4 turn potentiometer and a Lambda Regulated Power Supply (Model LP410 FM). As the motor turned the wavelength control, it also turned the potentiometer, thus sending a voltage to the plotter that was proportional to the wavelength. The scanning rate was 2.2 nm/sec.

3.7 Determination of the Photon Flux of the Xenon Lamp

The spectral distribution of the xenon lamp was determined at the sample position so the photoconductivity spectra can be normalized to a constant photon flux. Details concerning the measurement are given in Appendix B.

IV. Results and Discussion

4.1 Optical Absorption of Gamma-Irradiated LiF

The optical absorption spectra of LiF were measured in the spectral range of 700 nm to 200 nm. The optical absorption spectra were measured with unpolarized light and light polarized in the [011] and [0$\bar{1}$1] directions relative to the crystal axis at temperatures of 90 °K and 300 °K.

Figures 10 through 13 show the optical absorption spectra of Harshaw or Optovac LiF versus photon energy after exposure to 0.066 Mrad of gamma irradiation. It can be seen that the F-center absorbance in the Optovac sample is approximately twice as large as the F-center absorbance in the Harshaw sample for the same dose. Rabin observed in NaCl that the initial concentration of negative ion vacancies is larger in Optovac samples than in Harshaw samples[4]. By the introduction of $CaCl_2$ to NaCl, the concentration of negative ion vacancies increases causing a greater F-center absorbance upon irradiation[4,7,27]. Neutron Activation Analysis on the LiF samples in this study indicated that the Optovac LiF contained a higher concentration of an alkaline earth impurity than the Harshaw LiF which could explain the larger F-center absorbance in the Optovac samples.

By decreasing the temperature of the LiF samples from 300 °K to 90 °K, the F-center optical absorption shifts to higher energy. The F-center absorption peak shifts from 5.0 eV to 5.1 eV. The decrease in sample temperature also increases the height and reduces the full-width at half maximum (FWHM) of the F-center absorption band. The FWHM of the F-center absorption band decreases from 0.8 eV at 300 °K to 0.6 eV at 90 °K in Harshaw LiF, and from 1.0 eV at 300 °K to 0.7 eV at 90 °K in Optovac LiF.
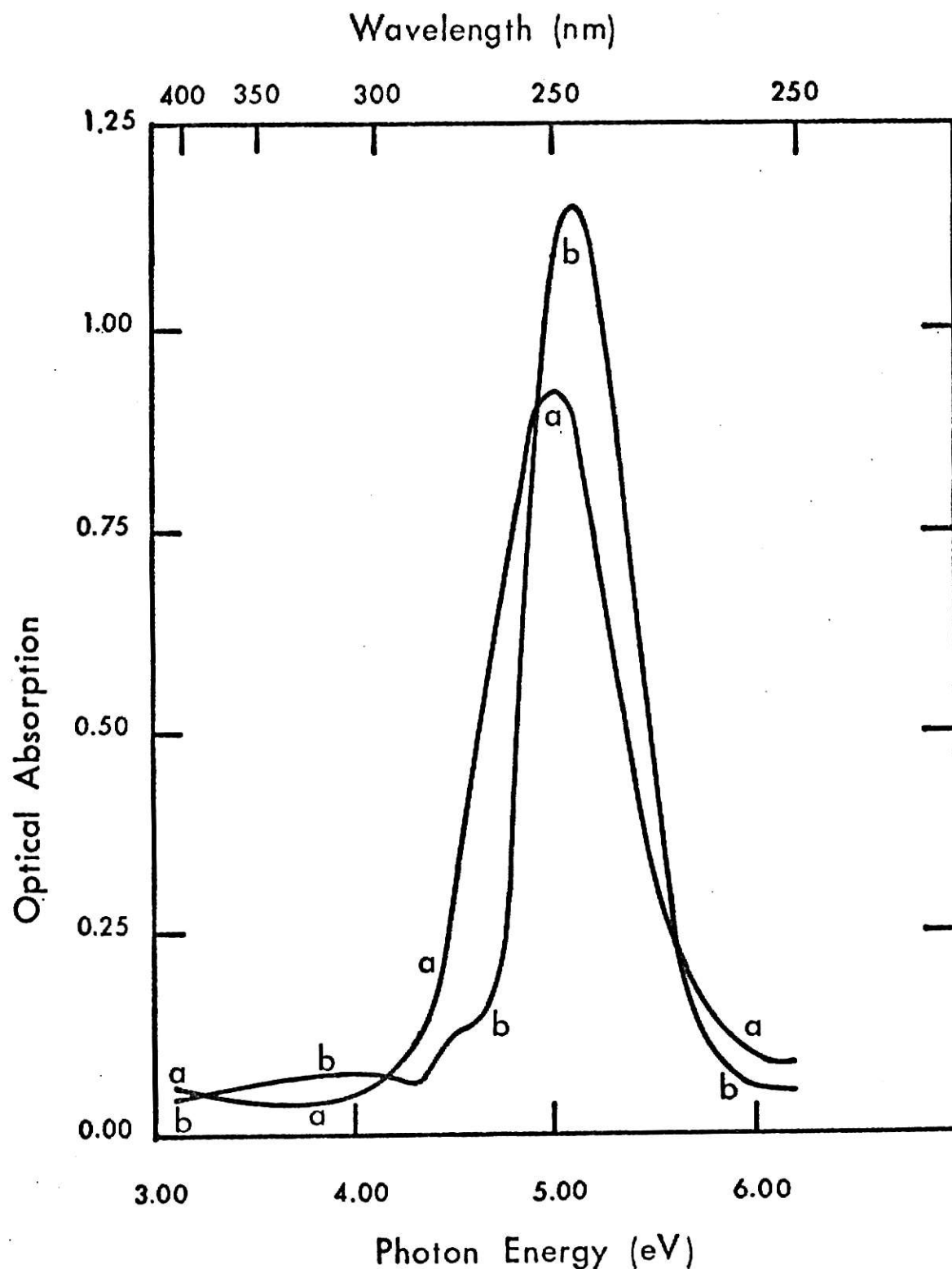
FIGURE 10: Optical absorption spectra of irradiated Harshaw LiF measured with unpolarized light at 90 °K and 300 °K. Curve (a) is the optical absorption spectrum measured at 300 °K. Curve (b) is the optical absorption spectrum measured at 90 °K. Absorbed Dose = 0.066 Mrad.

FIGURE 11: Optical absorption spectra of irradiated Harshaw LiF measured with [011] and [0$\bar{1}$1] polarized light at 90 °K. Curve (a) is the optical absorption spectrum measured with [011] polarized light. Curve (b) is the optical absorption spectrum measured with [0$\bar{1}$1] polarized light. Absorbed Dose = 0.066 Mrad.
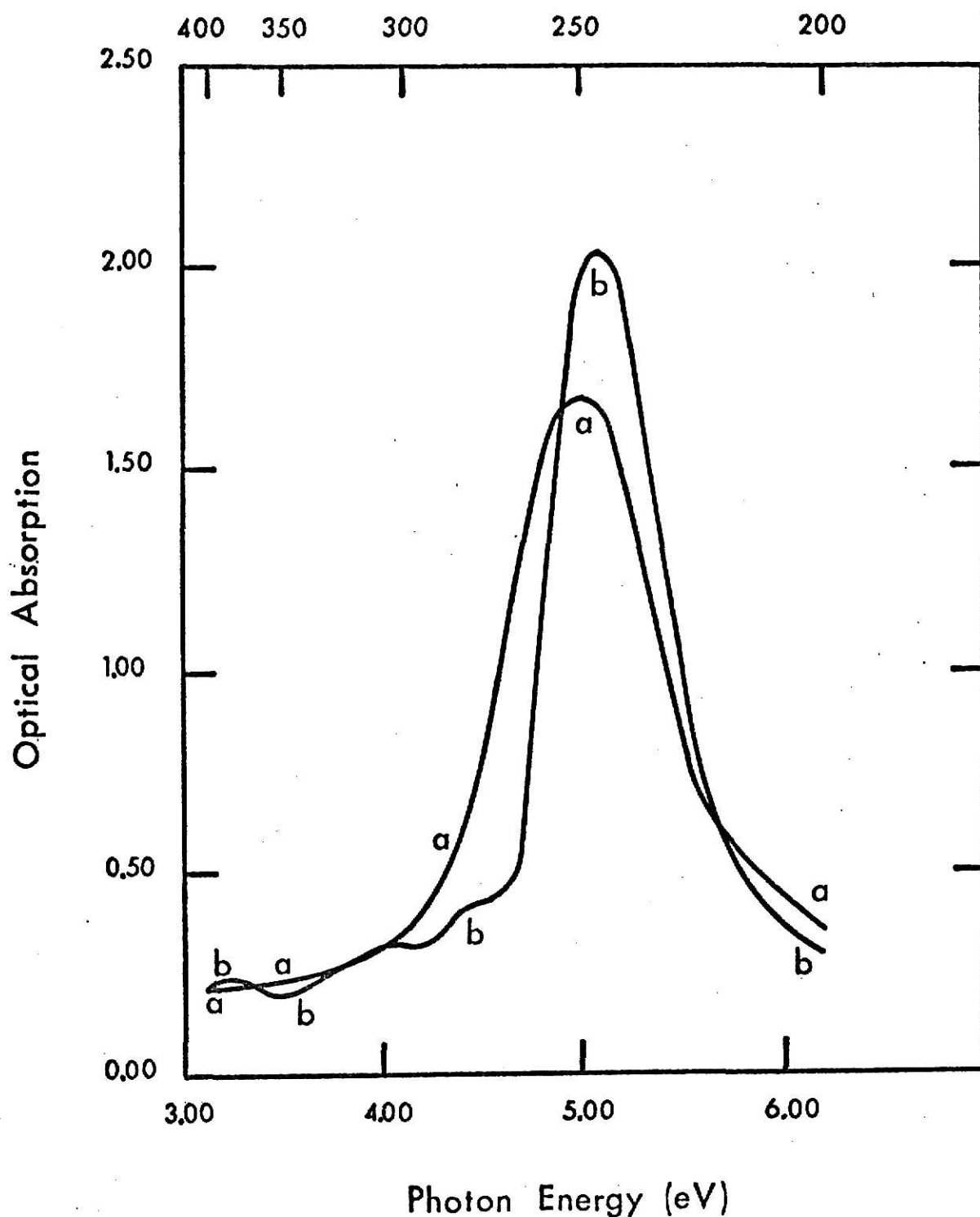
FIGURE 12: Optical absorption spectra of irradiated Optovac LiF measured
with unpolarized light at 90 °K and 300 °K. Curve (a) is the
optical absorption spectrum measured at 300 °K. Curve (b) is
the optical absorption spectrum measured at 90 °K. Absorbed
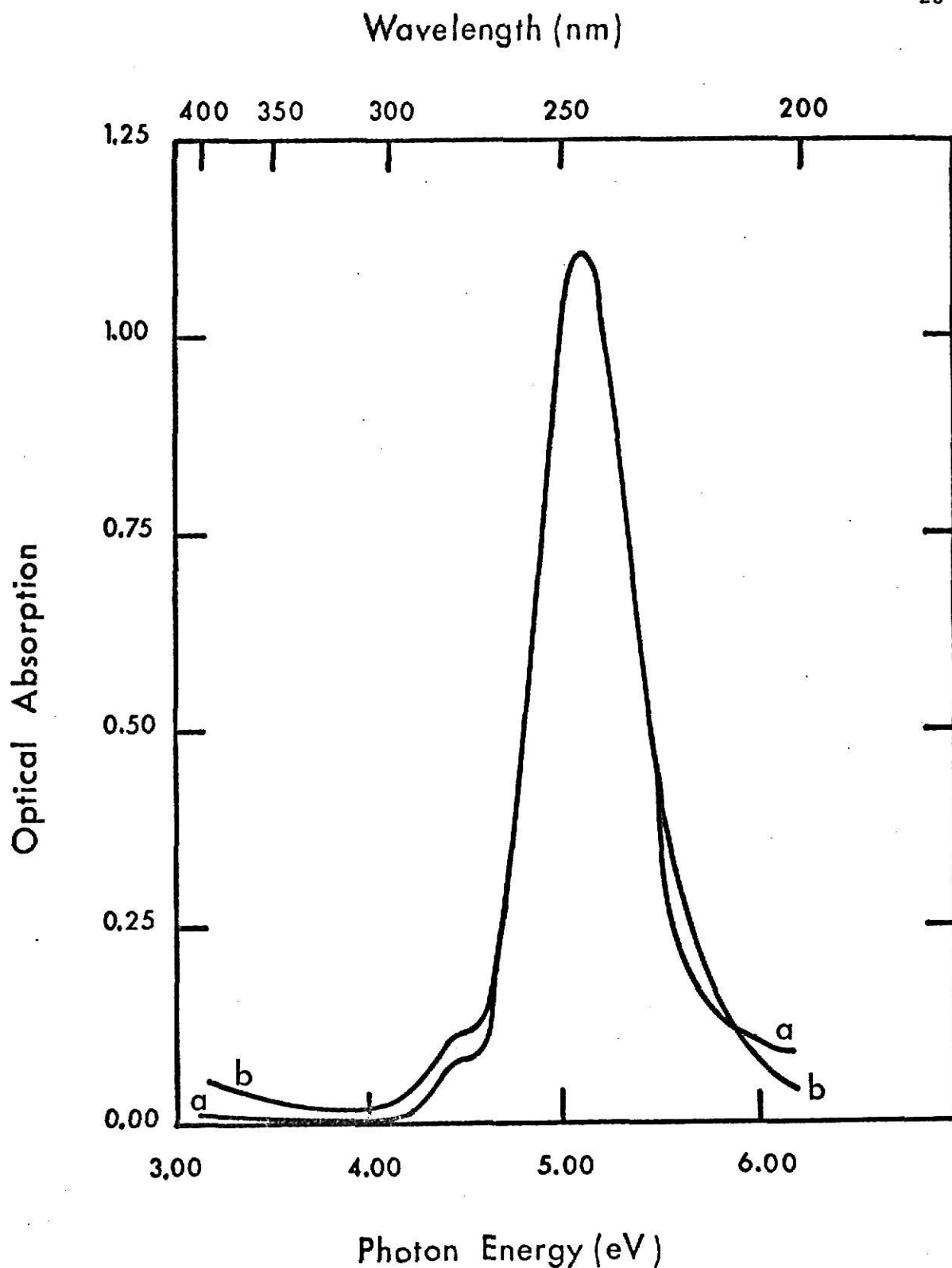Dose = 0.066 Mrad.
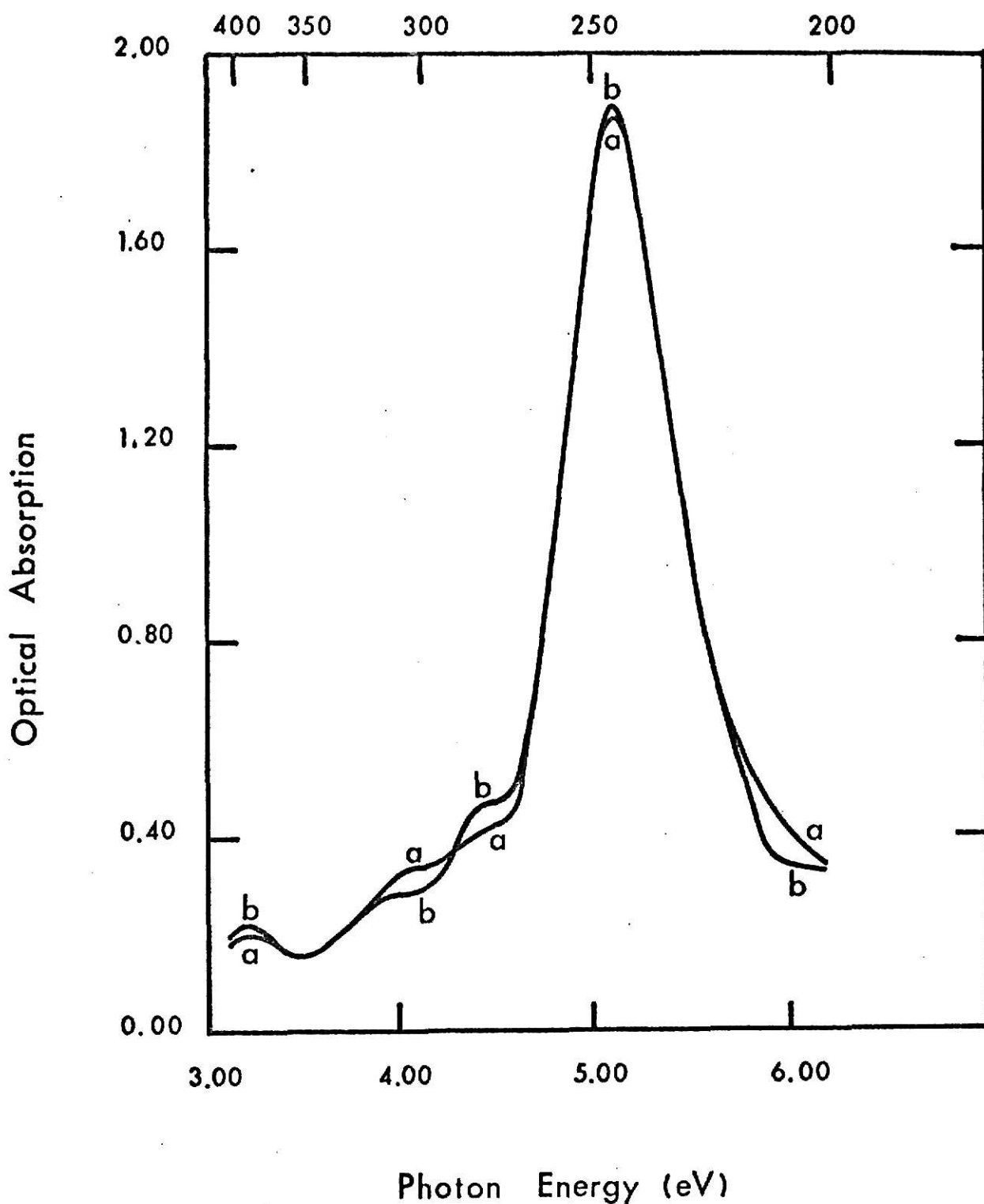
FIGURE 13: Optical absorption spectra of irradiated Optovac LiF measured with [011] and [0$\bar{1}$1] polarized light at 90 °K. Curve (a) is the optical absorption spectrum measured with [011] polarized light. Curve (b) is the optical absorption spectrum measured with [0$\bar{1}$1] polarized light. Absorbed Dose = 0.066 Mrad.

The shift in the F-center absorption peak can be qualitatively explained by the particle-in-a-box model of the F-center. The model states that the difference in energy levels of the particle in a box, which in this case is the F-center electron, is inversely proportional to the square of the size of the box. So, decreasing the temperature of the sample will decrease the size of the box by thermal contraction of the crystal lattice. The reduction in the box size will increase the difference between energy levels, and consequently the F-center absorption peak will shift to higher energies.

The narrowing of the FWHM of the F-center absorption band can also be qualitatively explained by the particle-in-a-box model of the F-center. The FWHM of the absorption band arises from the thermal vibrations of the neighboring ions, which in this case are Li^{+1} ions, surrounding the F-center. The amplitude of the vibration will give a range of possible values for the size of the box. Since the amplitude of this vibration is a function of temperature, the amplitude of the vibration will decrease as the temperature decreases. A decrease in the amplitude of the vibration will result in a smaller range for the possible values of the size of the box, and thus decrease the FWHM of the F-center absorption band.

Figures 10, 11, 12, and 13 show the optical absorption spectra measured at 90 °K with polarized and unpolarized light. The spectra not only contain a prominent F-center absorption band, but also an unresolved absorption band on the low energy side of the F-center absorption band around 4.4 eV. This unresolved absorption band is not seen at 300 °K. The absorption band has been observed before in work conducted by Mehta and Marrs on LiF[18,28] and has been labeled as the Y-center by Marrs[18].

Marrs observed the Y-center at both 90 °K and 300 °K with polarized and unpolarized light with crystals obtained in 1972 from Harshaw Chemical Corporation.

The Y-center exhibited dichroic behavior; the concentration of Y-centers oriented in the [0$\bar{1}$1] direction was larger than the concentration of Y-centers oriented in the [011] direction[18], as shown on Figs. 11 and 13. At this time there is no explanation why the dichroic behavior is exhibited by the Y-center.

Marrs proposed a model of the Y-center which involves an interstitial positive ion impurity adjacent to an F-center[18]. Neutron Activation Analysis run on the Harshaw samples used in Marrs work (1972 crystals) and in this work (1975 crystals) indicated aluminum as the common impurity, at a concentration of 22.5 ppm in the 1972 samples and 2.5 ppm in the 1975 samples. This impurity concentration difference could possibly explain why the Y-center is not seen at 300 °K in the present work.

Figures 11 and 13 indicate the absorbance of the Y-center compared to that of the F-center is about 20% in the Optovac sample, and 10% in the Harshaw sample. The Optovac sample contains a greater Y-center concentration than the Harshaw sample. Neutron Activation Analysis on the LiF samples indicated aluminum as the common impurity, and the concentration of aluminum was found to be slightly greater in the Optovac sample. The Y-center may have a greater probability of occurring in the Optovac LiF because it (Optovac LiF) contains a greater concentration of F-centers and a greater concentration of the common impurity (aluminum).

Figures 12 and 13 show two areas of increased absorption in the Optovac LiF absorption spectra around 3.2 eV and 4.0 eV. Mehta observed these absorption bands in his work on magnesium doped LiF. Mehta proposed that these bands are due to trapped electron centers similar to the Z-type centers observed in other alkali halides doped with alkaline-earth impurities[28]. Neutron Activation Analysis indicated that the Optovac samples contained a magnesium impurity, at a concentration of 32.0 ppm.

4.2 Effect of Optical Bleaching on the Optical Absorption Spectra

Optical absorption samples were bleached with either unpolarized light or light polarized in the [011] and [0$\bar{1}$1] directions. Optical bleaching was performed at 300 °K and 90 °K. At 300 °K, the samples were bleached with wavelengths of 254 nm or 280 nm. At 90 °K, the samples were bleached with wavelengths of 244 nm or 280 nm. The maximum absorption of the F-center in LiF occurs at 254 nm and 244 nm at 300 °K and 90 °K, respectively. Most of the optical bleaching was performed at 90 °K because the Y-center is observed at this temperature, whereas, it cannot be clearly seen in the optical absorption spectra at 300 °K.

Marrs optically bleached LiF (1972 cyrstals) at 300 °K with unpolarized light at 254 nm for 930 minutes. The result of the optical bleach was a decrease in the Y-center optical absorption measured with [0$\bar{1}$1] polarized light and an increase in the Y-center optical absorption measured with [011] polarized light. The Y-center optical absorption for the two polarizations were equal after the optical bleach. Marrs also optically bleached LiF (1972 crystals) at 90 °K with [011] polarized light at 244 nm for 90 minutes. The results observed for this optical bleach were the same that were observed for the 300 °K bleach. The dichroism of the Y-center was not observed and the Y-center optical absorptions for the two polarizations were equal[18].

Optical bleaching was performed under the following conditions:

1)   with [011] polarized light at 254 nm at 300 °K for 90 minutes,

2)   with [011] polarized light at 280 nm at 300 °K for 90 minutes,

3)   with [011] polarized light at 244 nm at 90 °K for 90 minutes,

4)   with [011] polarized light at 280 nm at 90 °K for 90 minutes.

Bleaching at any of the above conditions had no effect on the LiF optical

absorption. Longer periods of optical bleaching were used with unpolarized light to see if a bleaching effect could be observed. Optical bleaching was performed with unpolarized light at 244 nm at 90 °K for 300 minutes, and with unpolarized light at 280 nm at 90 °K for 300 minutes.

The effect of bleaching on the optical absorption of Harshaw LiF with unpolarized light at 244 nm at 90 °K for 300 minutes is shown in Figs. 14 and 15. Figure 14a is the optical absorption measured with [011] polarized light and Fig. 15a is the optical absorption measured with [0$\bar{1}$1] polarized light before the optical bleach. Figures 14b and 15b are the respective optical absorption spectrum measured after the bleach. From Figs. 14b and 15b it is observed that the Y-center optical absorption measured with [0$\bar{1}$1] polarized light and [011] polarized light both decreased to make the optical absorption of the Y-center approximately equal for the two polarizations after the optical bleach. The decrease in the Y-center absorption measured with [0$\bar{1}$1] polarized light is greater than the decrease measured with [011] polarized light.

The effect of bleaching on the optical absorption of Optovac LiF with unpolarized light at 244 nm at 90 °K for 300 minutes is shown in Figs. 16 and 17. Figure 16a is the optical absorption measured with [011] polarized light and Fig. 17a is the optical absorption measured with [0$\bar{1}$1] polarized light before the optical bleach. Figures 16b and 17b are the respective optical absorption spectrum measured after the bleach. For both polarizations, the Y-center optical absorption has decreased and the Y-center optical absorption after the optical bleach is approximately equal, similar to the observations on Harshaw LiF.

FIGURE 14: Optical absorption spectra of irradiated Harshaw LiF measured with [011] polarized light at 90 °K before and after an optical bleach with unpolarized light at 90 °K. Curve (a) is the optical absorption spectrum before the bleach. Curve (b) is the optical absorption spectrum after a 300 minute bleach at 244 nm. Absorbed Dose = 0.066 Mrad.
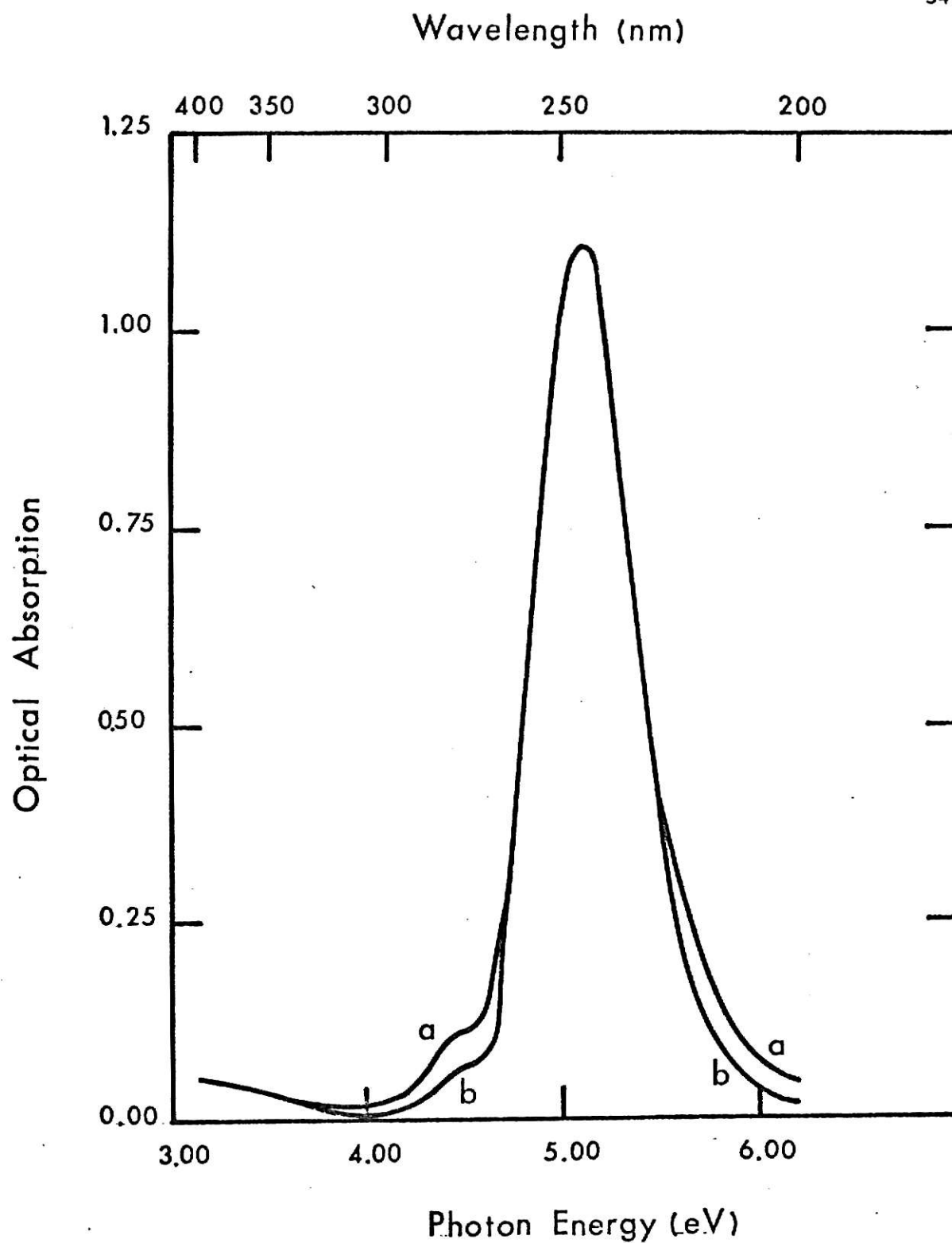
FIGURE 15: Optical absorption spectra of irradiated Harshaw LiF measured with [0Ī1] polarized light at 90 °K before and after an optical bleach with unpolarized light at 90 °K. Curve (a) is the optical absorption spectrum before the bleach. Curve (b) is the optical absorption spectrum after a 300 minute bleach at 244 nm. Absorbed Dose = 0.066 Mrad.
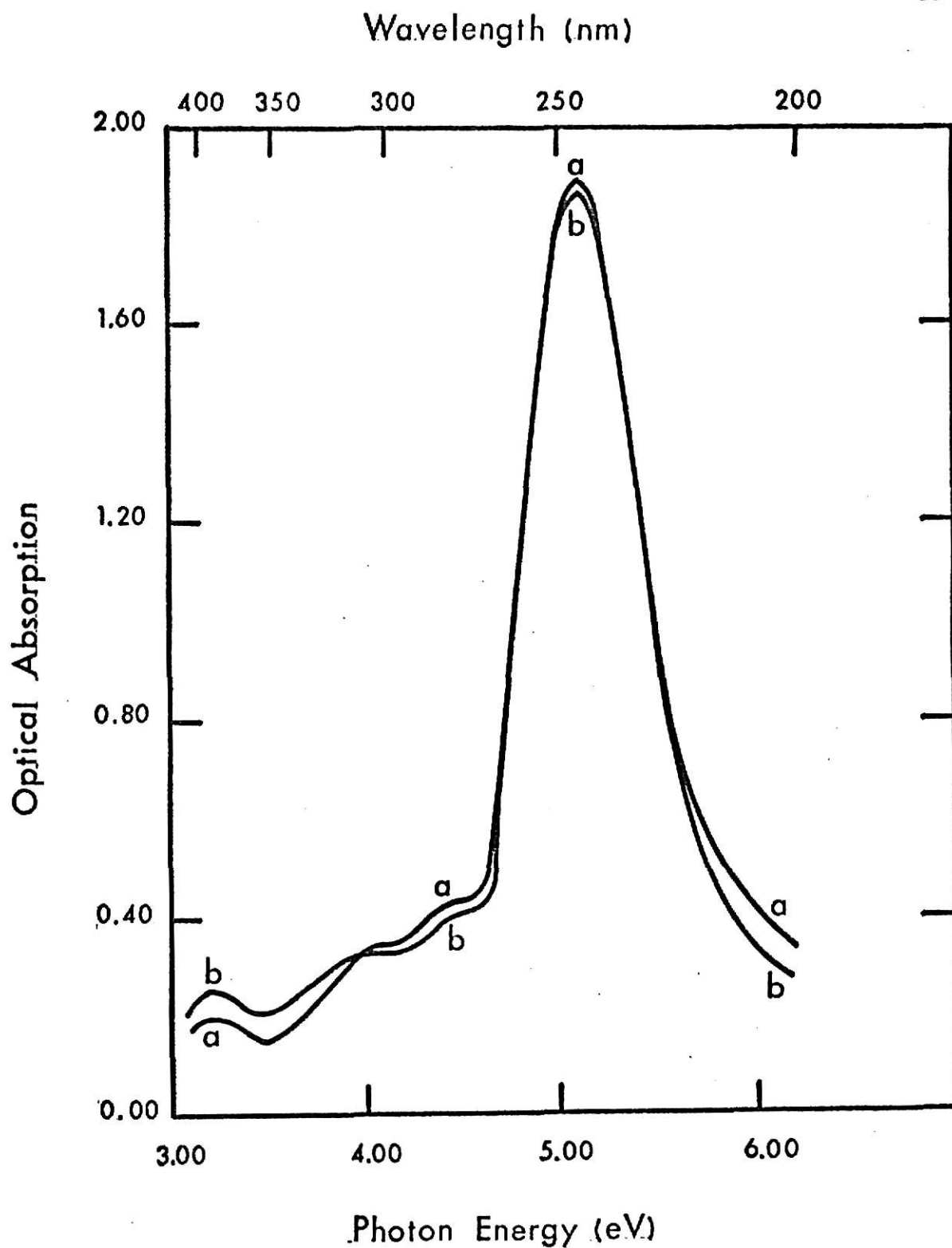
FIGURE 16: Optical absorption spectra of irradiated Optovac LiF measured with [011] polarized light at 90 °K before and after an optical bleach with unpolarized light at 90 °K. Curve (a) is the optical absorption spectrum before the bleach. Curve (b) is the optical absorption spectrum after a 300 minute bleach at 244 nm. Absorbed Dose = 0.066 Mrad.
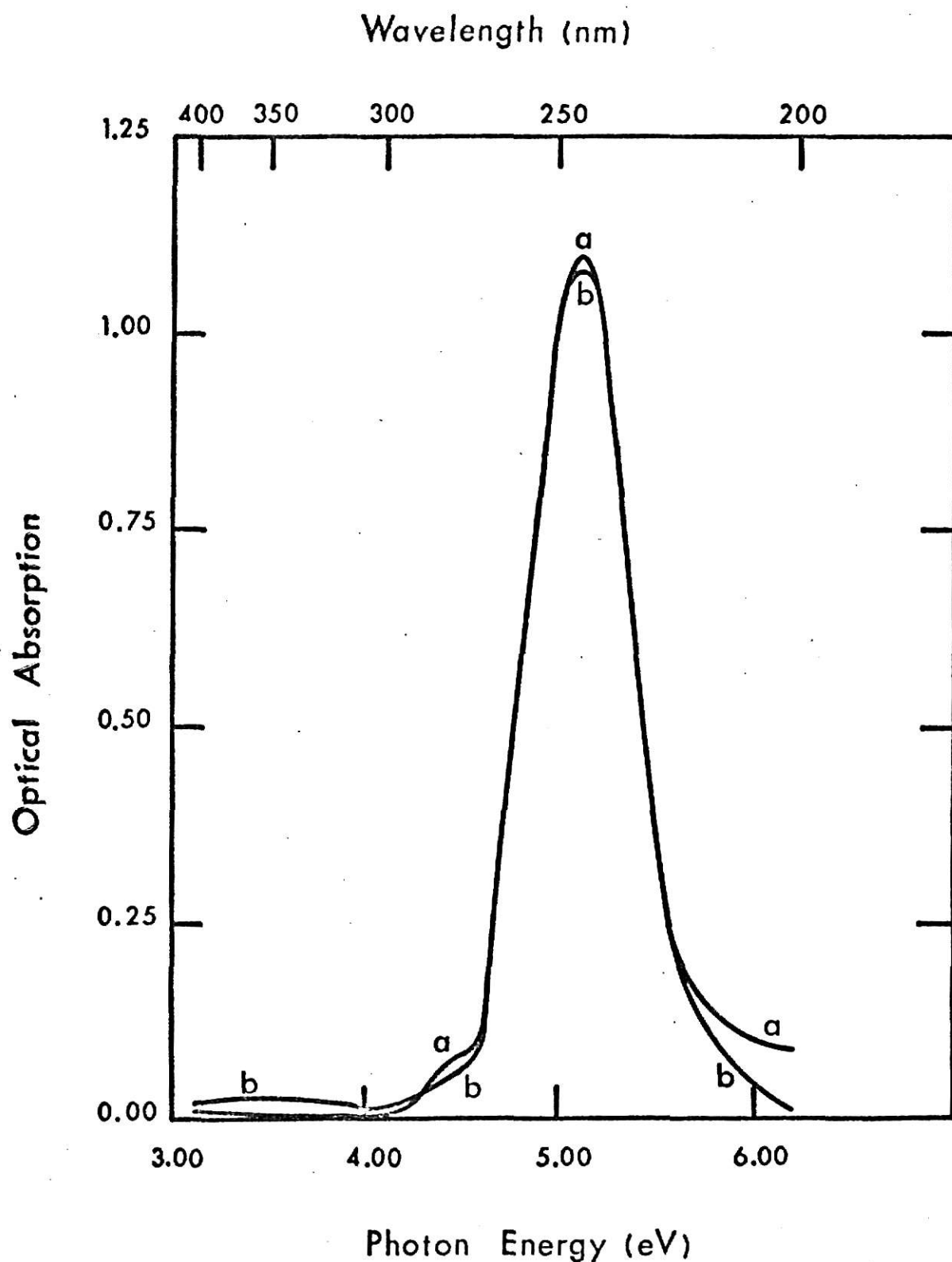
FIGURE 17: Optical absorption spectra of irradiated Optovac LiF measured with [0$\bar{1}$1] polarized light at 90 °K before and after an optical bleach with unpolarized light at 90 °K. Curve (a) is the optical absorption spectrum before the bleach. Curve (b) is the optical absorption spectrum after a 300 minute bleach at 244 nm. Absorbed Dose = 0.066 Mrad.
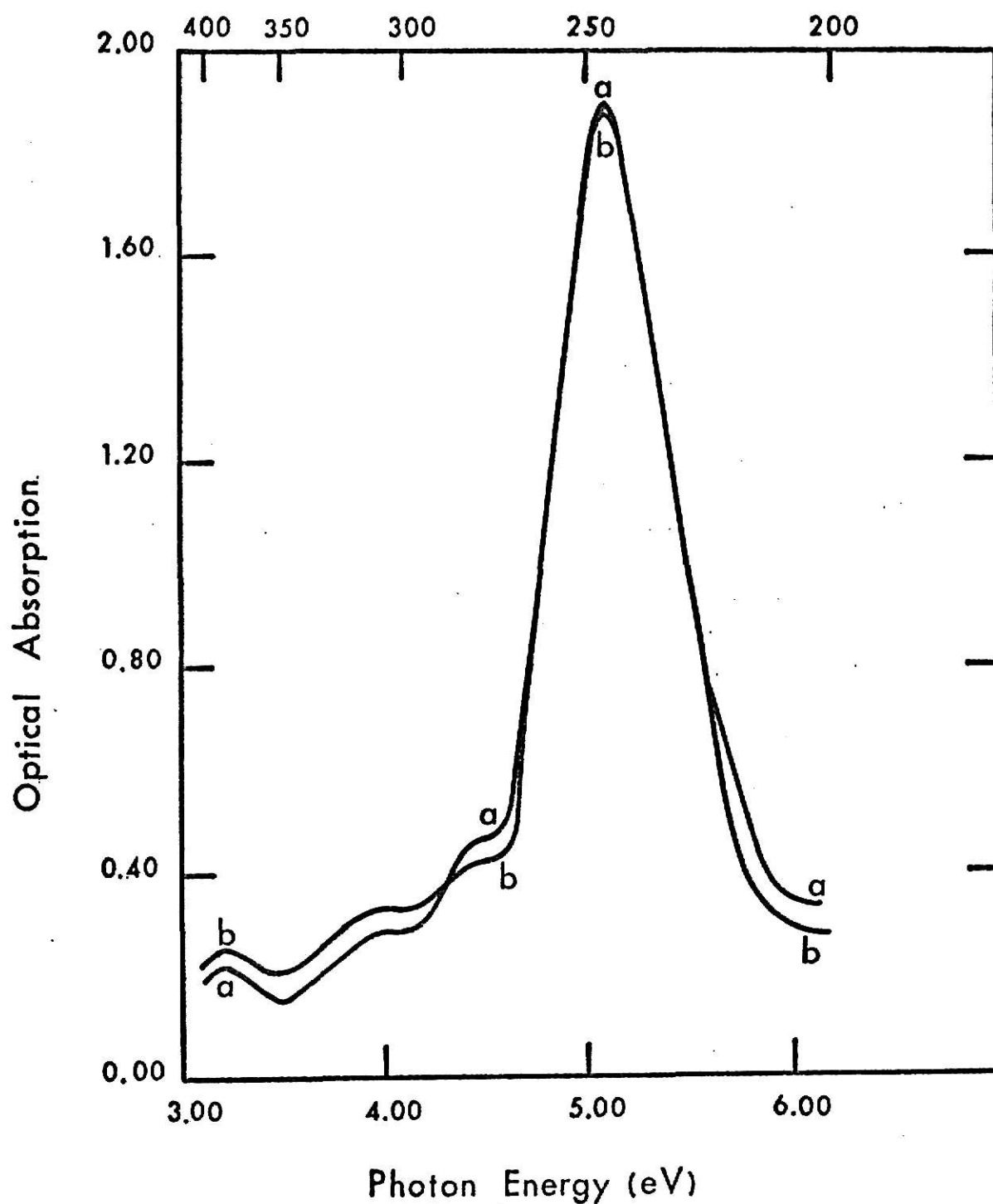
For both polarizations in both samples of LiF, the optical bleaching at 244 nm has decreased the population of the Y-center. This indicates that an F-center like optical transition is associated with the Y-center.

Optical bleaching with unpolarized light at 280 nm at 90 °K for 300 minutes had no effect on the optical absorption. Optical bleaching performed with light polarized in the [011] direction at 244 nm at 90 °K for 300 minutes, and with [0$\bar{1}$1] polarized light at 244 nm at 90 °K for 300 minutes also had no effect on the optical absorption.

The difference in the bleaching effect and bleaching rate that exists between Marrs' work and this work can possibly be due to the concentration of impurities in the samples. As mentioned previously, the samples Marrs used in his work (1972 crystals) contained more impurities, and at greater concentrations, than the samples used in this work (1975 crystals). The common impurity in the three samples was aluminum.

4.3 Photoconductivity of Irradiated LiF

The photoconductivity excitation spectra of LiF were measured in the spectral range of 370 nm to 200 nm as a function of dose and as a function of temperature. The output of the xenon lamp is not constant from 370 nm to 200 nm (see Appendix B). All photoconductivity excitation spectra were normalized to a constant photon flux. The photoconductivity excitation spectra were measured with unpolarized light and light polarized in the [011] and [0$\bar{1}$1] directions relative to the crystal axis at the following temperatures; 85 °K, 128 °K, 171 °K, 214 °K, 257 °K, and 300 °K. The absorbed dose varied from 0.007 Mrad to 0.7 Mrad.

Figure 18 shows the photoconductivity excitation spectrum before normalization of Harshaw LiF for unpolarized light at 300 °K prior to irradiation.

Wavelength (nm)

Photon Energy (eV)

FIGURE 18: Dark current spectrum and photoconductivity excitation plus dark current spectrum prior to normalization of unirradiated Harshaw LiF measured with unpolarized light at 300 °K. Curve (a) is the dark current spectrum. Curve (b) is the photoconductivity excitation plus dark current spectrum.

Figure 18a is the dark current spectrum and Fig. 18b is the photoconductivity excitation plus dark current spectrum. The photoconductivity excitation spectrum on the unirradiated sample is obtained by subtracting the dark current spectrum (Fig. 18a) from the photoconductivity excitation plus dark current spectrum (Fig. 18b). The dark current will be discussed in the following section. Figure 18b indicates a photocurrent peak at approximately 5.05 eV (246 nm). Nelson observed this peak in his work on unirradiated LiF[13].

Figure 19 shows the photoconductivity excitation spectrum before normalization of Harshaw LiF for unpolarized light at 300 °K for an absorbed dose of 0.7 Mrad. Figures 19a and 19b are once again the dark current spectrum and photoconductivity excitation plus dark current spectrum, respectively. A prominent photocurrent peak is seen at 4.38 eV (283 nm), and the peak previously observed on the unirradiated spectrum at 5.05 eV (246 nm) is not seen.

Figure 20 shows the normalized photoconductivity excitation spectra for the spectra in Figs. 18 and 19. Figure 20a is the photoconductivity excitation spectrum for unirradiated LiF and Fig. 20b is the photoconductivity excitation spectrum for irradiated LiF. After normalization, it can be seen on Fig. 20a that the photocurrent peak at 5.05 eV does not exist. An increase in the photocurrent occurs at higher photon energies which may indicate the presence of another defect center which may be photoconductive. It is questionable as to how much of the photocurrent increase is real, because the intensity of the xenon lamp decreases very rapidly in this region, making the normalization difficult (see Appendix B). The irradiation has decreased the photocurrent seen at higher photon energies causing it to shift from its original position in the unirradiated spectrum. The unirradiated spectrum is then fitted to the irradiated spectrum, as shown by the dashed line in Fig. 20. Subtraction of the shifted
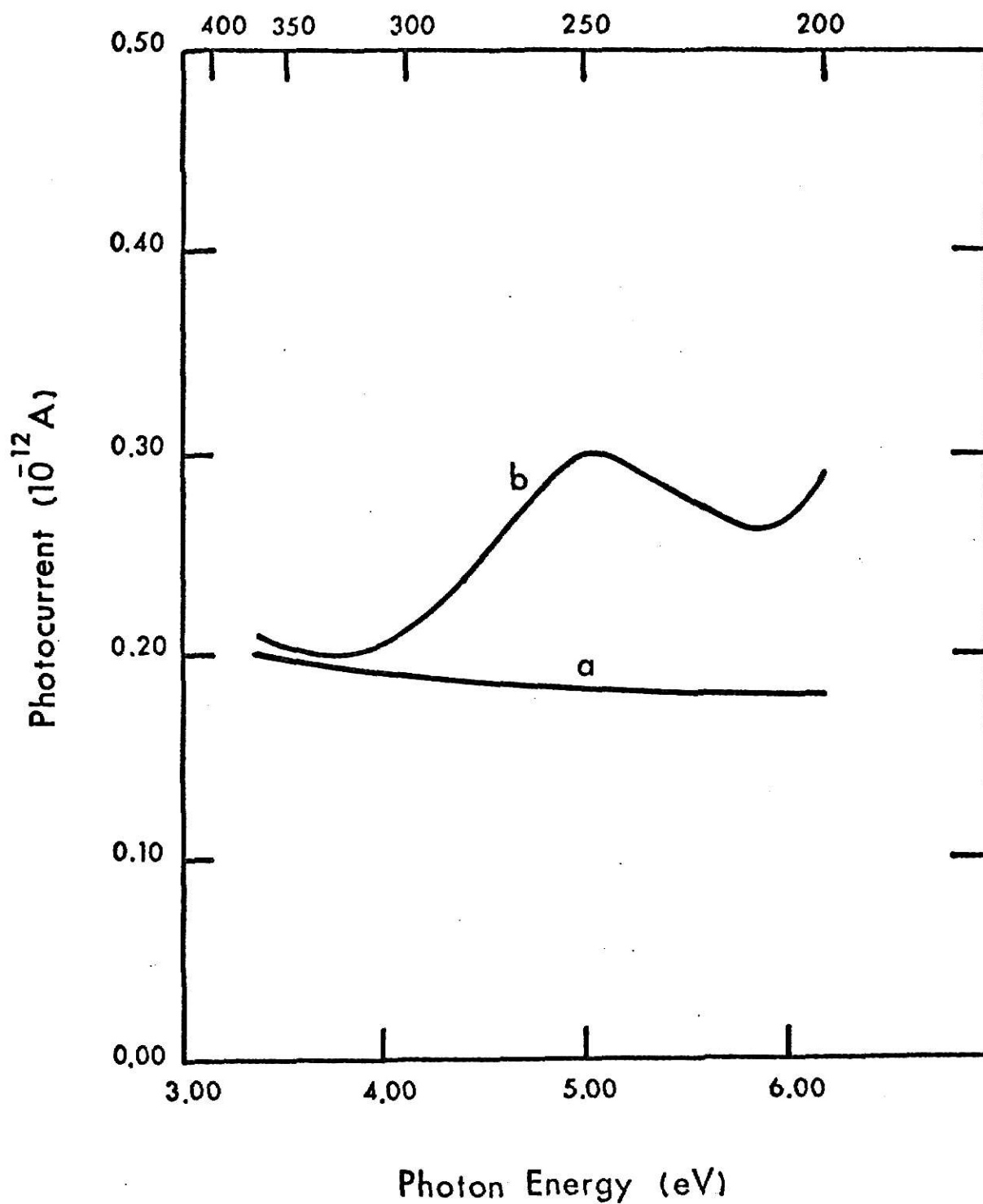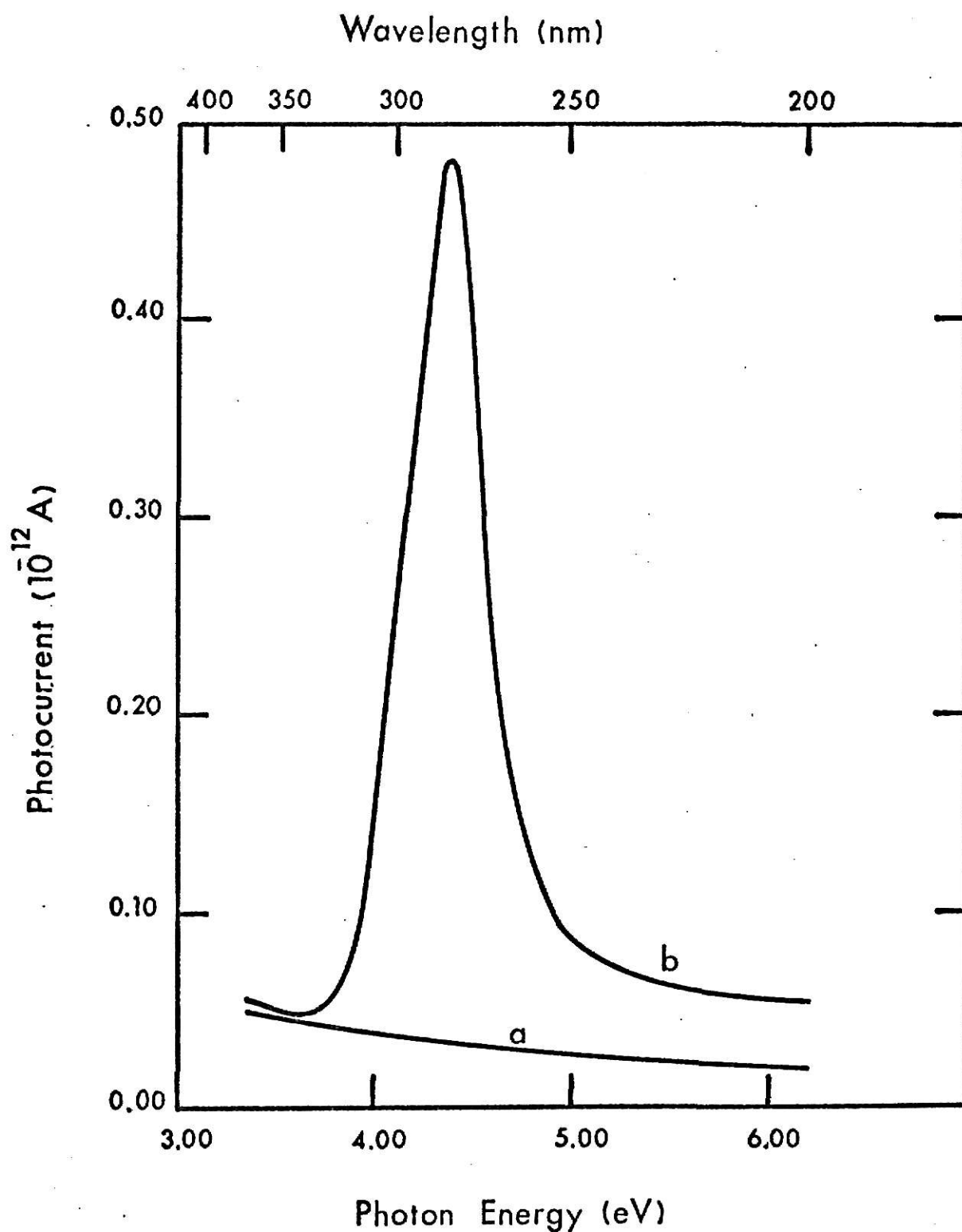
FIGURE 19: Dark current spectrum and photoconductivity excitation plus dark current spectrum prior to normalization of irradiated Harshaw LiF measured with unpolarized light at 300 °K. Curve (a) is the dark current spectrum. Curve (b) is the photoconductivity excitation plus dark current spectrum. Absorbed Dose = 0.7 Mrad.

FIGURE 20: Normalized photoconductivity excitation spectra of unirradiated and irradiated Harshaw LiF measured with unpolarized light at 300 °K. Curve (a) is the unirradiated spectrum. Curve (b) is the irradiated spectrum. Absorbed Dose = 0.7 Mrad.

unirradiated spectrum (dashed line) from the irradiated spectrum (Fig. 20b) gives the photocurrent peak due to gamma irradiation as shown in Fig. 21. The photocurrent peak occurs at 4.47 eV (277 nm) which is approximately at the same energy where the Y-center absorption band was observed.

Figures 22 and 23 show the photoconductivity excitation spectra of Harshaw and Optovac LiF, respectively, for unpolarized light at various temperatures for an absorbed dose of 0.70 Mrad. For both samples, the decrease in temperature from 257 °K to 85 °K shifts the photocurrent peak position to higher energy, decreases the FWHM of the photocurrent peak, increases the area under the photocurrent peak, and increases the peak height. The photocurrent peak exhibits qualitatively the same behavior as the F-center absorption band for decreasing temperature, except for the increase in the area under the photocurrent peak.

The shift of the photocurrent peak position to higher energy can be explained by the same arguments given for the shift of the F-center optical absorption band (see Section - Optical Absorption of Irradiated LiF). Marrs found in his work that the FWHM of the photocurrent peak follows the same temperature dependence as the FWHM of the F-center absorption band in LiF[18].

The increase in the peak height and an increase in the area under the photocurrent peak with decreasing temperature can be understood by examining the two terms that contribute to a change in the conductivity; density of free charge carriers and mobility of the free carriers.

The density of free charge carriers is a function of production rate and mean lifetime of the carrier in the free state. Marrs concluded in his work that the production rate of free carriers does not account for the observed changes in peak height and area under the photocurrent peak in the temperature range used for photoconductivity measurements[18].
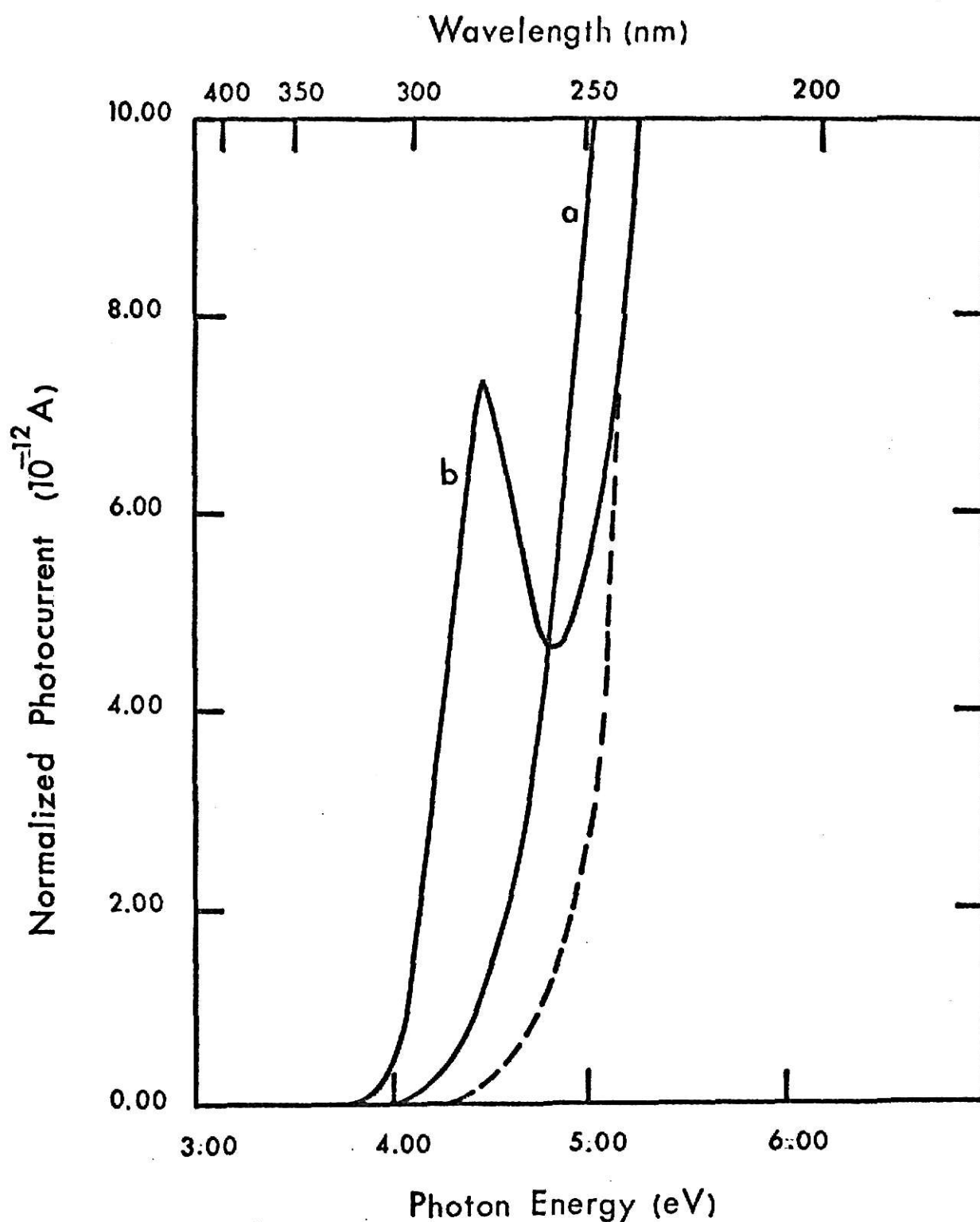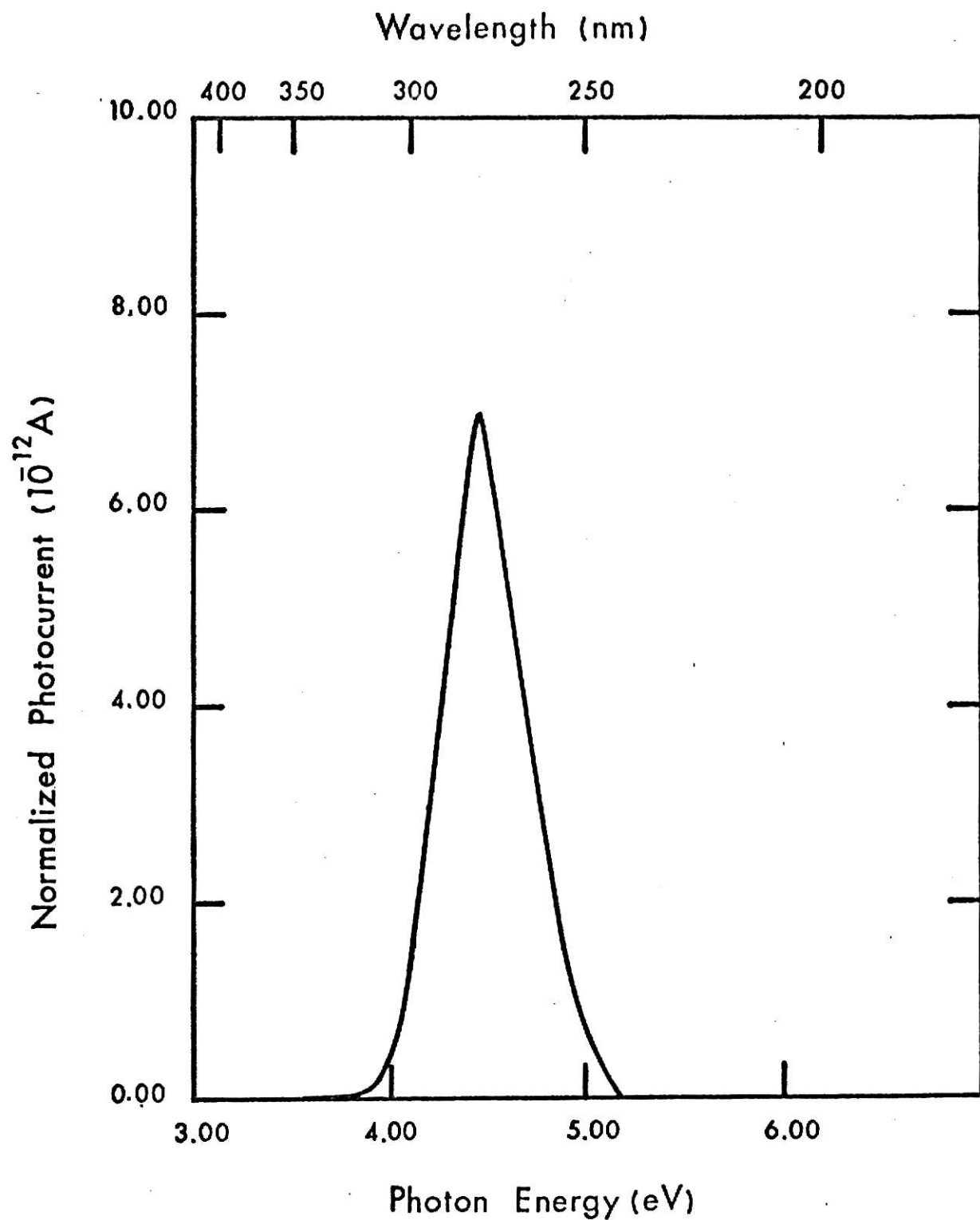
FIGURE 21: Normalized photoconductivity excitation spectrum of irradiated Harshaw LiF measured with unpolarized light at 300 °K. Absorbed Dose = 0.7 Mrad.

FIGURE 22: Normalized photoconductivity excitation spectra of irradiated Harshaw LiF measured with unpolarized light at 85 °K, 171 °K, and 257 °K. Curves (a), (b), and (c) are the normalized photoconductivity excitation spectra measured at 85 °K, 171 °K, and 257 °K, respectively.
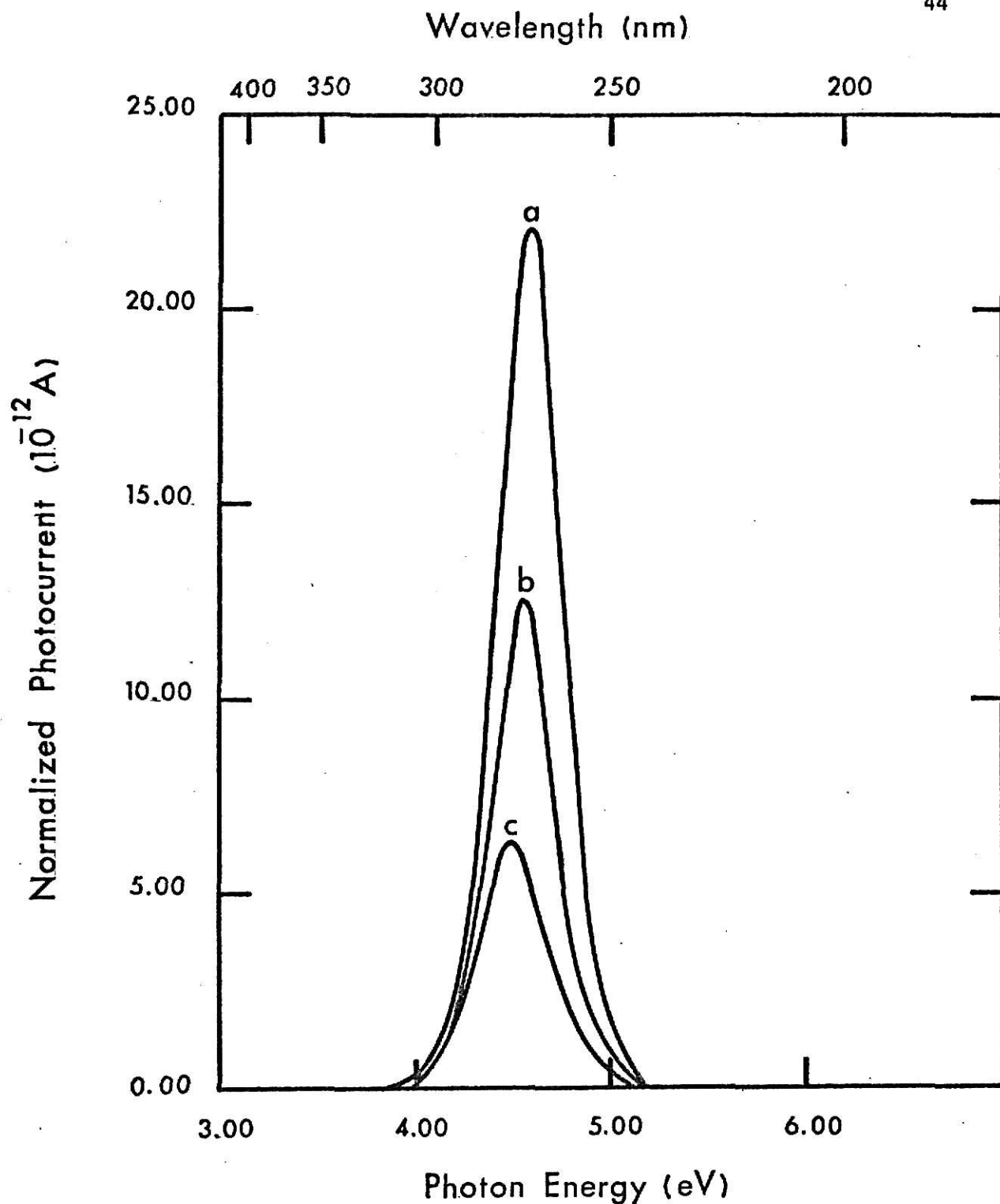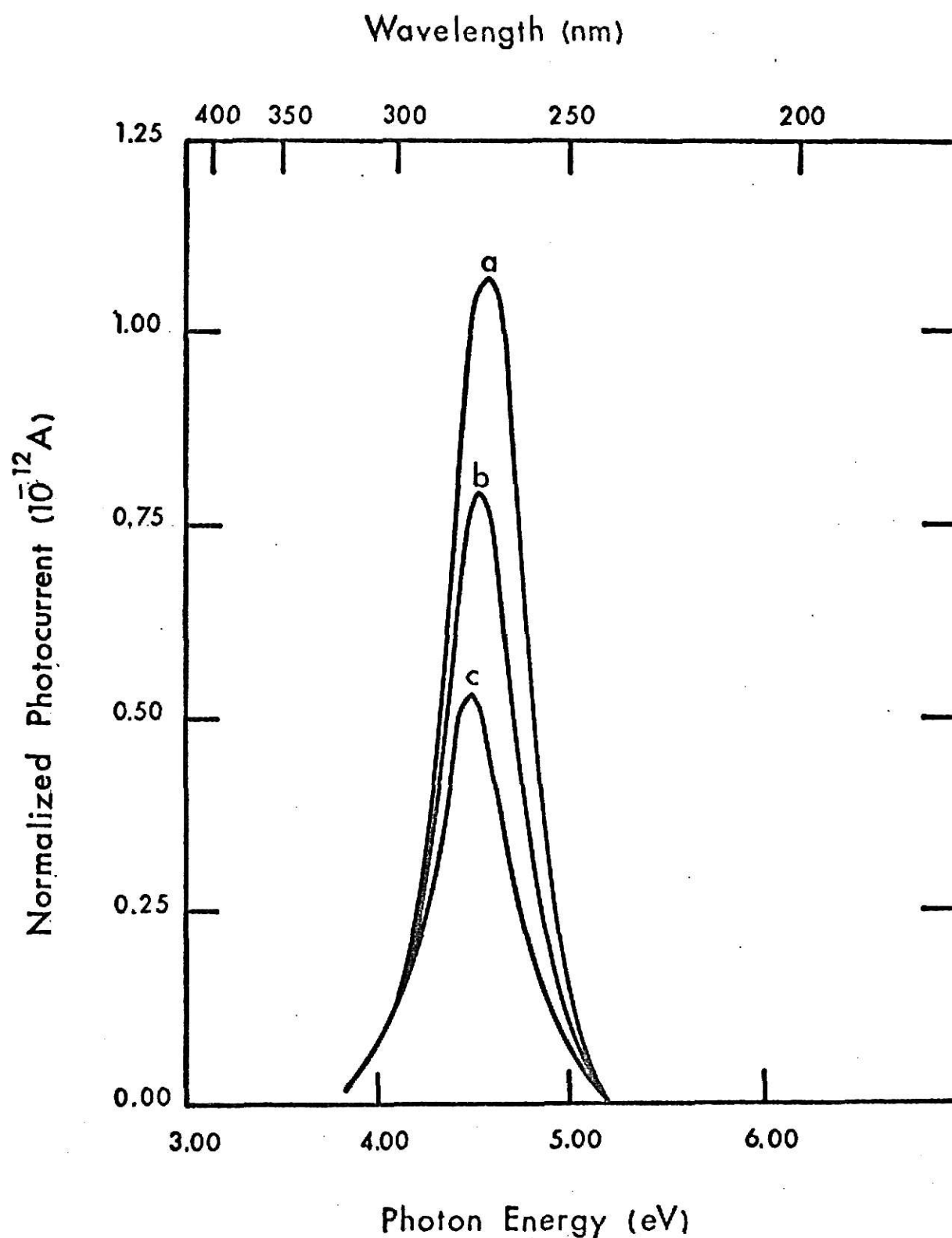
FIGURE 23: Normalized photoconductivity excitation spectra of irradiated Optovac LiF measured with unpolarized light at 85 °K, 171 °K, and 257 °K. Curves (a), (b), and (c) are the normalized photoconductivity excitation spectra measured at 85 °K, 171 °K, and 257 °K, respectively.

The mean lifetime of the carrier depends upon the mechanisms which govern the rates of carrier removal from and emission into the conduction band and how these mechanisms vary with temperature. Since the area under the photocurrent peak increases with a decrease of temperature, this indicates that the mechanisms governing the removal of free carriers from the conduction band have changed in such a way as to increase the carrier lifetime. The specifics of the change are presently unknown.

The other contributor to conductivity change is a change in the mobility of the free carriers. The mobility of the free charge carriers increases with decreasing temperature because the mobility is limited at low temperatures by scattering from impurities, whereas, at high temperature scattering occurs from optical phonons[7,24].

From Figs. 22 and 23, it is also seen that in Harshaw LiF the photocurrent is larger than in Optovac LiF. A possible explanation for the photocurrent difference is the impurity difference between the two crystals. Optovac LiF contains more impurities, and at greater concentrations, which will create more defects and scattering centers to limit the photoconductivity in the sample.

Tables 1 and 2 contain some of the data received from photoconductivity excitation measurements run on Harshaw and Optovac LiF, respectively. The variation of photocurrent peak height as a function of dose at various temperatures is shown in Figs. 24 and 25 for Harshaw and Optovac LiF, respectively. The variation of photocurrent peak area as a function of dose at various temperatures is shown in Figs. 26 and 27 for Harshaw and Optovac LiF, respectively. At this time, the reason for the difference in behavior exhibited between the Optovac and Harshaw LiF is unknown.

TABLE 1

Harshaw Data

Temperature (°K)	Photocurrent Peak Position (nm)	Photocurrent Peak Magnitude $(\times 10^{-12} \pm 0.002 \times 10^{-12})A$	Normalized Photocurrent Peak Area
For a dose of 0.70 Mrad			
85	270	22.00	1.000
128	271	16.93	0.726
171	272	12.46	0.590
214	274	8.33	0.405
257	276	6.27	0.305
300	278	6.93	0.370
For a dose of 0.20 Mrad			
85	269.5	3.32	0.162
128	273	1.93	0.090
171	272	1.86	0.102
214	274	1.47	0.075
257	277	1.11	0.062
300	277.5	1.09	0.056
For a dose of 0.07 Mrad			
85	270	2.61	0.131
128	269	2.44	0.132
171	270.5	1.96	0.099
214	273	1.40	0.070
257	275	1.08	0.055
300	276	1.00	0.058

TABLE 2

Optovac Data

Temperature (°K)	Photocurrent Peak Position (nm)	Photocurrent Peak Magnitude $(\times 10^{-12} \pm 0.002 \times 10^{-12})$A	Normalized Photocurrent Peak Area
For a dose of 0.70 Mrad			
85	269	1.14	1.00
128	270	1.07	0.99
171	273.5	0.77	0.69
214	274.5	0.53	0.63
257	275	0.53	0.49
300	278.5	0.51	0.47
For a dose of 0.20 Mrad			
85	271	1.08	0.87
128	273	0.75	0.62
171	273	0.60	0.49
214	274	0.48	0.40
257	275.5	0.50	0.45
300	279	0.27	0.26
For a dose of 0.07 Mrad			
85.	269	0.84	0.72
128	269	0.89	0.74
171	270	0.54	0.43
214	273	0.42	0.38
257	277.5	0.25	0.22
300	278.5	0.23	0.26

FIGURE 24: Normalized photocurrent as a function of dose of Harshaw LiF measured at 85 °K, 171 °K, and 257 °K. Curves (a), (b), and (c) are the normalized photocurrent measured at temperatures of 85 °K, 171 °K, and 257 °K, respectively.

FIGURE 25: Normalized photocurrent as a function of dose of Optovac LiF measured at 85 °K, 171 °K, and 257 °K. Curves (a), (b), and (c) are the normalized photocurrent measured at temperatures of 85 °K, 171 °K, and 257 °K, respectively.

FIGURE 26: Normalized photocurrent peak area as a function of dose of Harshaw LiF measured at 85 °K, 171 °K, and 257 °K. Curves (a), (b), and (c) are the normalized photocurrent peak area measured at temperatures of 85 °K, 171 °K, and 257 °K, respectively.
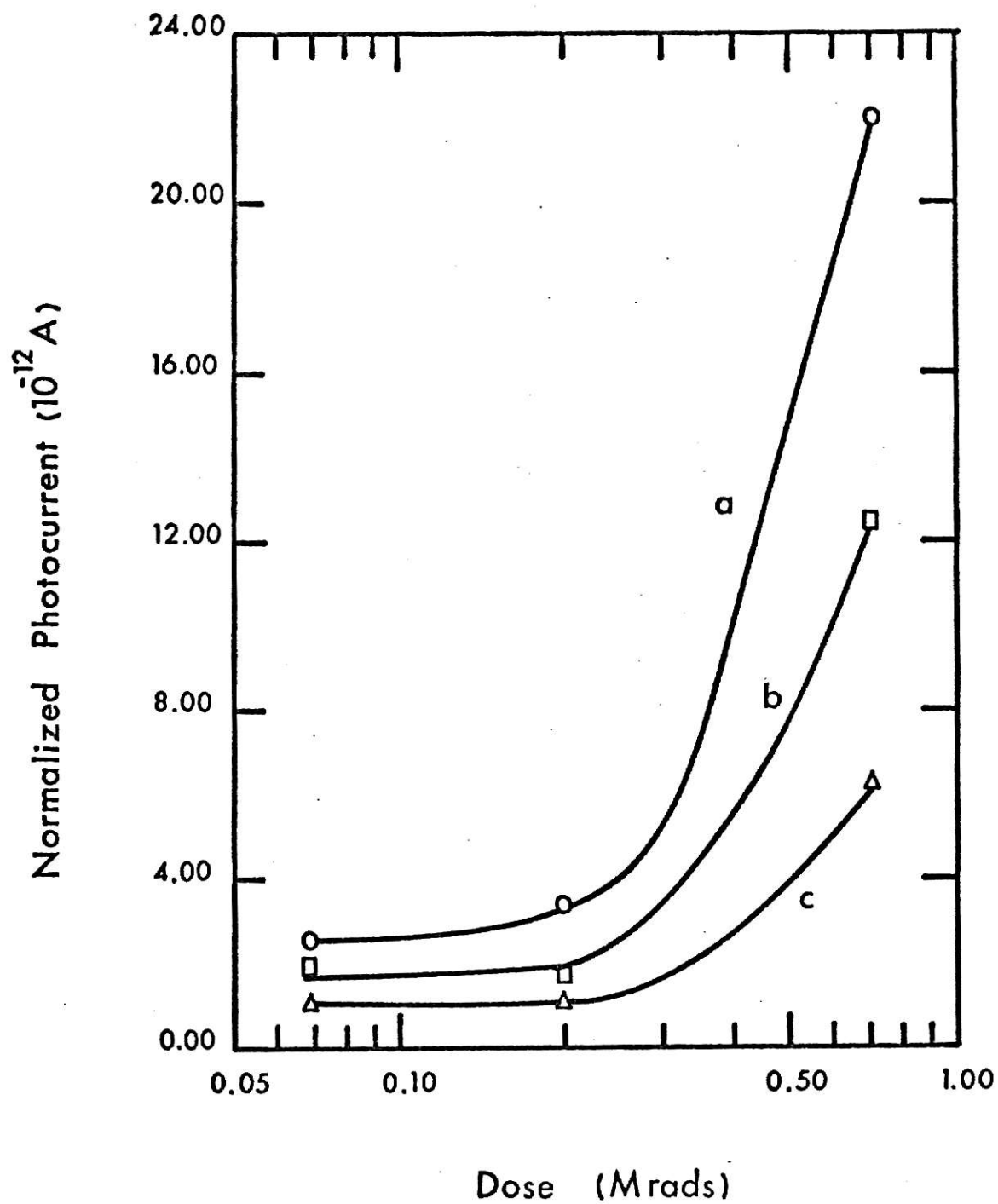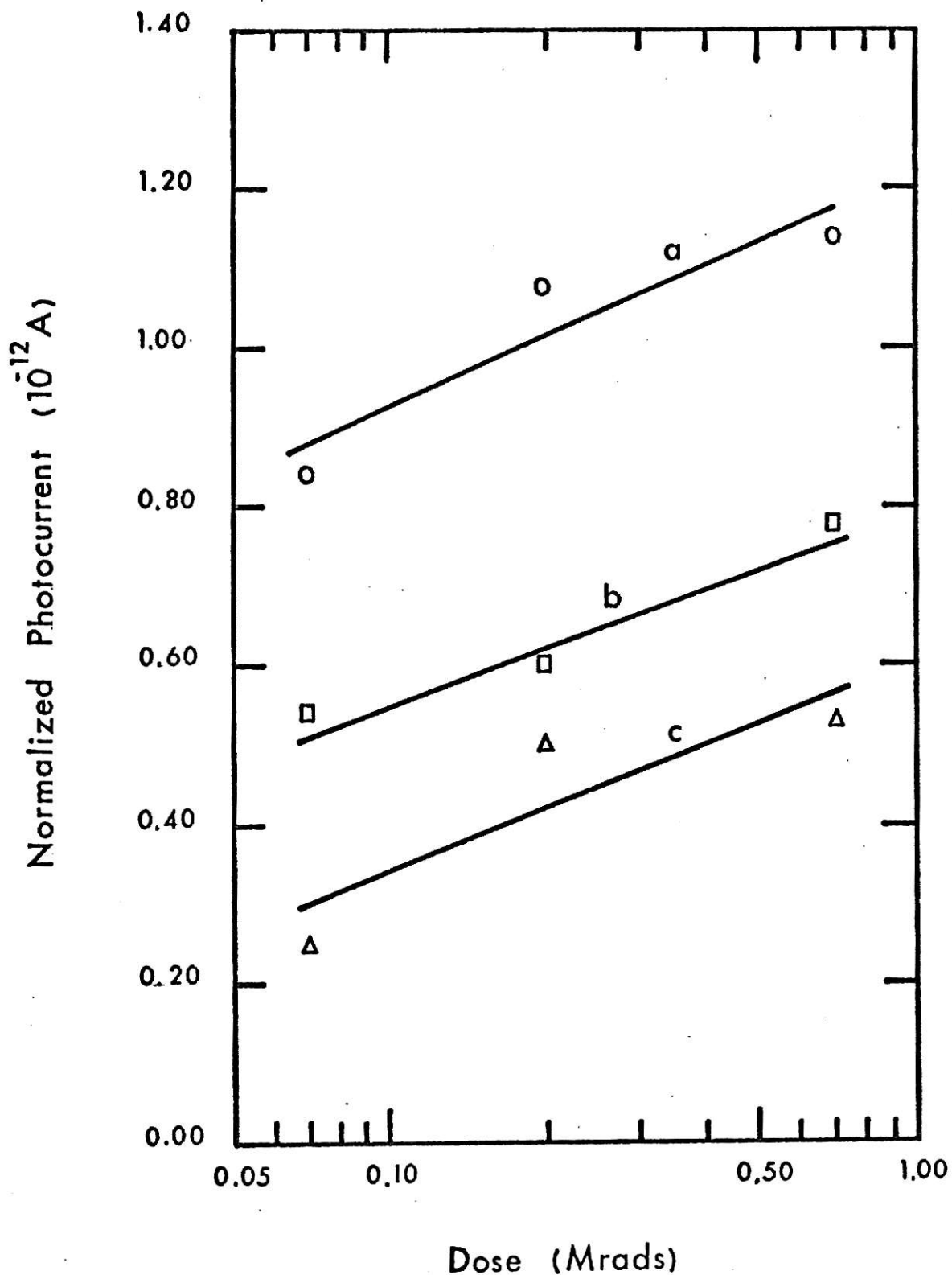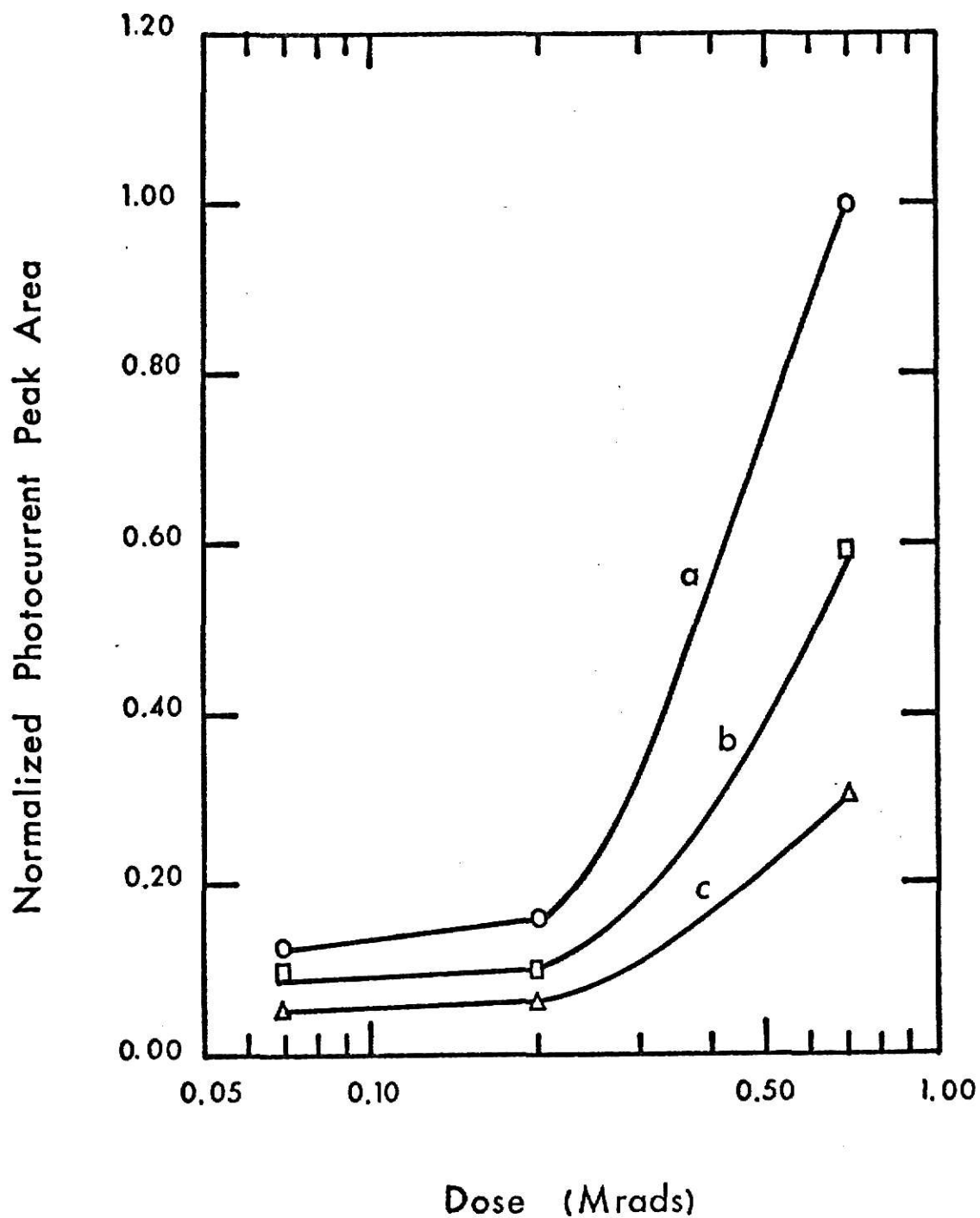
FIGURE 27: Normalized photocurrent peak area as a function of dose of Optovac LiF measured at 85 °K, 171 °K, and 257 °K. Curves (a), (b), and (c) are the normalized photocurrent peak area measured at temperatures of 85 °K, 171 °K, and 257 °K, respectively.
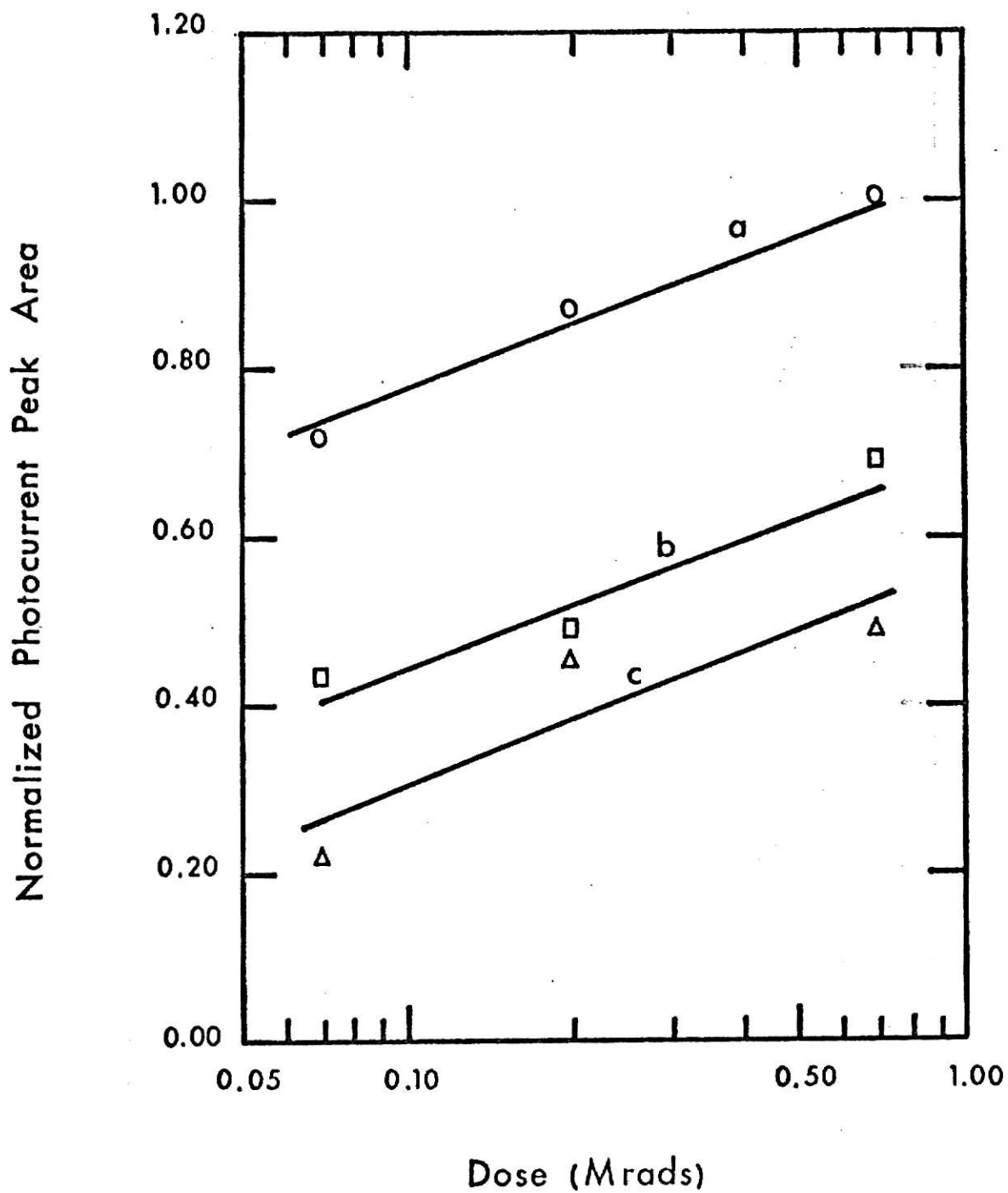
The photoconductivity measurements indicate that the photocurrent peak position does not shift with increasing dose at any one given temperature. In a previous work, Nelson observed that the photocurrent peak shifted to longer wavelengths with increasing dose at 300 °K[13]. This apparent shift occurred because the photoconductivity excitation spectra were not normalized to a constant photon flux.

4.4 Dark Current of Irradiated LiF

Figures 18a and 19a show the dark current spectra of unirradiated and irradiated Harshaw LiF, respectively. The dark current is created by application of an electric field, -1000 volts bias voltage, to the sample. Impurities, Frenkel defects, and Schottky defects under the influence of an applied electric field could produce a current[18,24]. The energy of activation for motion of Frenkel and Schottky defects in LiF are 1.3 eV and 1.9 eV, respectively[29].

The dark current is from one to two orders of magnitude smaller than the peak photocurrent in Harshaw and Optovac LiF. The dark current after irradiation is less than the dark current prior to irradiation, as shown on Figs. 18a and 19a. A decrease in sample temperature also decreases the magnitude of the dark current. The lowering of the temperature decreases the mobility because there is less thermal excitation.

It was also observed that Optovac LiF contained a larger dark current than Harshaw LiF. Since the Optovac samples contained more impurities than the Harshaw samples, there are more positive ion vacancies in the Optovac LiF.

4.5 Photoconductivity of Irradiated LiF with [011] and [0$\bar{1}$1] Polarized Light

Since the photocurrent band and absorption band are believed to be produced by the same defect, the Y-center, photoconductivity measurements were performed

with light polarized in the [011] and [01̄1] directions at temperatures between 85 °K and 300 °K to see if the dichroism of the absorption band was present in the photocurrent peak. Marrs ran photoconductivity measurements with [011] and [01̄1] polarized light at 300 °K and observed no dichroism[18]. In this work no dichroism was observed in Optovac LiF, but the results were inconclusive in Harshaw LiF. Further work must be done in this area.

4.6 A Model for the Y-center

The following is a summary of the observations that have been made during this work:

1) Optovac LiF contains a larger Y-center absorption band than Harshaw LiF at 90 °K which suggests that the Y-center is associated with an impurity atom or ion. The common impurity in both samples was aluminum, and Optovac LiF contained a slightly greater concentration.

2) The optical absorption band maximum of the Y-center occurs around 4.4 eV, approximately 0.6 eV below the maximum of the F-center absorption band at 5.0 eV. This is true for both Harshaw and Optovac LiF.

3) The Y-center absorption band can be optically bleached with un-polarized light at 244 nm at 90 °K which suggests the Y-center is associated with a F-center like optical transition.

4) The Y-center absorption band exhibits dichroism with respect to [011] and [01̄1] polarized light at 90 °K.

5) The photocurrent peak occurs approximately at the same energy as that of the Y-center absorption band, this indicates that both are produced by the same defects.

6) The photocurrent peak does not shift as the absorbed dose increases once the spectrum is normalized to a constant photon flux.

Marrs indicated that the Y-center is a perturbed F-center. The proposed model is shown in Fig. 28[18]. Since the Y-center appears in both Optovac and Harshaw LiF and the common impurity is aluminum, the interstitial is an aluminum ion.

The aluminum interstitial could produce the observed dichroism, but at this time it is unknown why the defect prefers the [0$\bar{1}$1] direction over the [011] direction. *Destruction of this defect requires the ejection of the electron from the defect upon absorption of a photon and thermal diffusion* of the aluminum interstitial to a neighboring site. The energy of activation of aluminum in LiF is unknown, but it is known that the energy of activation for motion of positive ion interstitials in several of the alkali halides is on the order of 0.1 eV[24,29]. Assuming that the energy of activation for aluminum in LiF is of the same magnitude, it is possible for thermal diffusion of the aluminum impurity at 90 °K.

The fact that the Y-center photocurrent peak is observed at 85 °K and that the Y-center absorption band is optically bleached at 90 °K indicates that the excited state of the Y-center is close to the conduction band. The Y-center is probably close enough to the conduction band to allow thermal ionization and promotion of the electron into the conduction band.
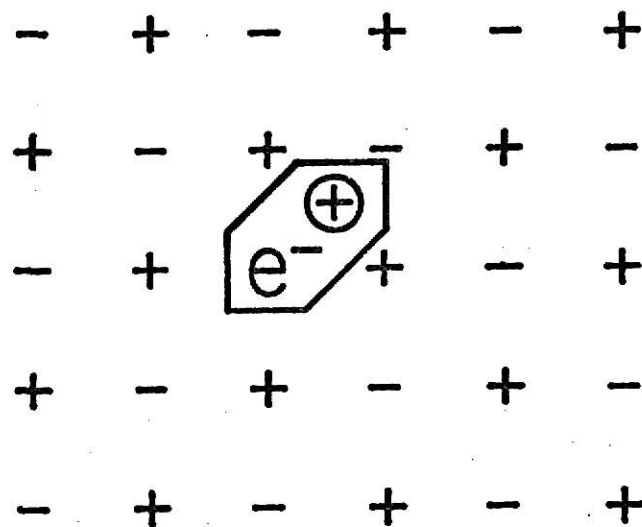
FIGURE 28: Proposed model of the Y-center, interstitial positive ion impurity adjacent to an F-center.

V. Summary and Conclusions

Optical absorption measurements performed on irradiated Harshaw and Optovac LiF samples with unpolarized light and light polarized in the [011] and [0$\bar{1}$1] directions indicated a dichroic absorption band (Y-center) on the low energy side of the F-center absorption band at 90 °K. The maximum of the Y-center absorption band is at approximately 4.4 eV. The dichroism indicates that the concentration of the Y-centers oriented in the [0$\bar{1}$1] direction is larger than the concentration of Y-centers oriented in the [011] direction. The mechanism that produces this dichroism is presently unknown. The Y-center absorption band in the Optovac samples was larger than in the Harshaw samples. The common impurity in both samples was aluminum, and the concentration of aluminum in the Optovac LiF was slightly greater than the concentration in the Harshaw LiF.

The Y-center absorption band can be optically bleached with unpolarized light at 244 nm at 90 °K. It is observed that the Y-center optical absorption measured with [0$\bar{1}$1] polarized light and [011] polarized light both decreased to make the optical absorption of the Y-center approximately equal for the two polarizations after the bleach. The decrease in the Y-center absorption measured with [0$\bar{1}$1] polarized light is greater than the decrease measured with [011] polarized light. This indicates that the population of the Y-center is decreasing as a result of the optical bleach. Since optical bleaching at 244 nm has decreased the population of the Y-center, this indicates that an F-center like optical transition is associated with the Y-center.

Photoconductivity excitation spectra of the Harshaw and Optovac LiF were measured with unpolarized light and light polarized in the [011] and [0$\bar{1}$1] directions at temperatures from 85 °K to 300 °K. A photocurrent peak due

to gamma irradiation is observed at 4.47 eV at 300 °K. Since the photocurrent

peak occurs at approximately the same energy as that of the Y-center absorption

band, this indicates that both are produced by the same defect. It is

observed for Optovac and Harshaw LiF that decreasing the temperature shifts

the photocurrent peak position to higher energy, decreases the FWHM of the

photocurrent peak, increases the area under the photocurrent peak, and in-

creases the peak height. The photocurrent peak exhibits qualitatively the same

behavior as the F-center absorption band for decreasing temperature, except for

the increase in the area under the photocurrent peak. The increases in the

area under the photocurrent peak and peak height is believed to be caused by an

increase in the mobility and mean lifetime of the electron with decreasing

temperature. It is also seen that the photocurrent peak does not shift as the

absorbed dose increases once the spectrum is normalized to a constant photon

flux.

Based on the results observed in this work, an expansion of a previously

proposed model for the Y-center is made. The model involves an interstitial

aluminum impurity adjacent to an F-center.

Areas of further work should include more photoconductivity excitation

measurements with polarized light to see if the dichroism of the absorption

band is present in the photoconductivity peak. Also, optical absorption

and photoconductivity measurements should be made with LiF doped with varying

concentrations of aluminum.

VI. References

1. S. C. Lind and D. C. Bardwell, "The Coloring and Thermophosphorescence Produced in Transparent Minerals and Gems by Radium Radiation," Am. Mineralogist 8, 171 (1923).

2. C. Doelter, "Coloration Obtained Under the Influence of Radium Rays," Lab. Mineral. 7, 58 (1911).

3. R. W. Pohl, "Electron Conductivity and Photochemical Processes in Alkali Halides," Proc. Phys. Soc. 49 (extra part), 3 (1937).

4. J. H. Schulman and W. D. Compton, Color Centers in Solids (Pergamon Press Book, MacMillan Company, Inc., New York, 1962), 1st ed., Vol. 2.

5. N. F. Mott and R. W. Gurney, Electronic Processes in Ionic Crystals (Clarendon Press, Oxford, 1940).

6. W. B. Fowler, Ed., Physics of Color Centers (Academic Press, New York, 1968).

7. J. J. Markham, F-centers in Alkali Halides (Academic Press, New York, 1966).

8. J. F. Merklin, lecture notes on Radiation Effects (Kansas State University).

9. A. Milgram and M. P. Givens, "Extreme Ultraviolet Absorption by Lithium Fluoride," Phys. Rev. 125, 1506 (1962).

10. R. H. Bube, Photoconductivity of Solids (John Wiley and Sons, Inc., New York, 1960).

11. R. S. Crandall, "Electron Capture by α and F centers in KBr," Phys. Rev. 138, A1242 (1965).

12. R. S. Crandall and M. Mikkor, "Photoconductivity of KBr Containing F Centers," Phys. Rev. 138, A1247 (1965).

13. W. E. Nelson, J. F. Merklin, and R. S. Lee, "Photoconductivity of Irradiated LiF," Nucl. Instrum. Methods 133, 387 (1976).

14. G. Wolfram, "Photoconductivity of the Z_2-Center in KCl:Sr Crystals," Phys. Status Solidi 28, K11-13 (1968).

15. G. R. Cole and R. J. Friauf, "Photoconductivity of Z Bands in KCl and an Associated New Band," Phys. Rev. 107, 387 (1957).

16. N. Inchauspe, "Photoconduction in KBr and KI Containing F Centers," Phys. Rev. 106, 898 (1957).

17. J. J. Oberly, "Photoconductivity of Trapped Electrons in KBr Crystals at Room Temperature," Phys. Rev. 84, 1257 (1951).

18. C. D. Marrs, A Study of the Optical Absorption and Photoconductivity of Gamma-Irradiated LiF, M.S. Thesis, Kansas State University (1976), unpublished.

19. P. D. Townsend and J. C. Kelly, Colour Centers and Imperfections in Insulators and Semiconductors (Crane, Russak and Company, Inc., New York, 1973).

20. E. Burstein and J. J. Oberly, "Optical Properties of F-centers at Liquid-Helium Temperatures," National Bureau of Standards Circular 519, 285 (1951).

21. T. Inui and Y. Uemura, "Theory of Color Centers in Ionic Crystals, II," Progr. Theoret. Phys. 5, 395 (1950).

22. P. Gorlich, Photoconductivity in Solids (Dover Publications Inc., New York, 1967).

23. A. Rose, Concepts in Photoconductivity and Allied Problems (Interscience Publishers, New York, 1963).

24. C. Kittel, Introduction to Solid State Physics (John Wiley and Sons, Inc., New York, 1966), 3rd ed.

25. P. Warmeck, "LiF Color Center Formation and UV Transmission Losses From Argon and Hydrogen Discharges," J. Opt. Soc. Am. 55, 921 (1965).

26. M. Kaiseruddin, Effects of Very High Dose Rates on the Response of LiF Thermoluminescent Dosimeters, M.S. Thesis, Kansas State University (1968), Bull. Am. Phys. Soc. 15, 1367 (1970).

27. H. Rabin, Phys. Rev. 116 (1959), Amer. Inst. Phys.

28. S. K. Mehta, Study of Optical Absorption Bands Responsible for Thermoluminescence of LiF:Mg, Ph.D. Dissertation, Kansas State University (1972), Bull. Am. Phys. Soc. 18, 311 (1973).

29. J. H. Crawford and L. N. Slifkin, Ed., Point Defects in Solids (Plenum Press, New York, 1972), 1st ed., Vol. 2.

30. N. D. Eckhoff, Optimal Neutron Activation Analysis, Ph.D. Dissertation, Kansas State University (1968).

31. "Operating Manual: L-101 Spectral Irradiance Standard and P-101 Current Supply," Electro Optics Associates, Palo Alto, California.

VII. Acknowledgements

Appendix A

Neutron Activation Analysis of LiF Samples

Neutron Activation Analysis was used to determine the atom concentrations of impurities of LiF crystals obtained from Optovac Chemical Corporation and Harshaw Chemical Corporation.

Neutron Activation Analysis depends upon the production of radioactive nuclei. The rate of formation of the radioactive nuclide, N, is given by

$$\overset{\circ}{N} = \sigma\phi N_o - \lambda N , \tag{A.1}$$

where N = the time dependent nuclide concentration,

$\overset{\circ}{N}$ = the derivative with respect to time,

N_o = the time dependent parent nuclide concentration,

σ = the microscopic activation cross section,

ϕ = the neutron flux,

λ = the decay constant.

The radioactive nuclei, which are directly proportional to the number of the parent nuclei, decay with the emission of gamma-rays.

If the neutron flux, ϕ, and time dependent parent nuclide concentration, N_o, are assumed to be constants, Eq. (A.1) has the following solution[30]:

$$N = \frac{\sigma\phi_o N_o}{\lambda} (1-e^{-\lambda t}) \tag{A.2}$$

where

N = time dependent nuclide concentration at time of removal from neutron flux,

t = time of exposure,

ϕ_o = neutron flux, a constant.

To determine the time dependent nuclide concentration after removal from the

neutron flux, the radioactive decay law is applied to Eq. (A.2), which gives

$$N = \frac{\sigma \phi_o N_o}{\lambda} (1-e^{-\lambda t}) \, e^{-\lambda \tau} \qquad (A.3)$$

where τ equals the time after removal from the neutron flux.

Qualitative neutron activation measurements were initially made to determine the impurity atoms in LiF. Small samples of LiF were placed in polyethylene vials and irradiated in the rotary specimen rack of the Kansas State University TRIGA Mk II nuclear reactor. After irradiation, activity (energy distribution) measurements were taken on a detection system which consisted of a Canberra Ge(Li) detector (Model 3000) and a Northern Scientific 636 pulse height analyzer.

Gamma rays with energies 0.845 and 1.782 MeV were detected. ^{28}Al has a 2.3 minute half-life and decays by beta emission accompanied by a 1.78 MeV gamma ray. ^{27}Mg has a 9.5 minute half-life and decays by beta emission accompanied predominantly by a 0.84 MeV gamma ray. The Optovac and Harshaw (1972 crystals) samples were found to contain aluminum and magnesium as impurities, and only aluminum was found in the 1975 Harshaw samples.

Quantitative neutron activation measurements were then made on the LiF crystals to determine the concentration of impurity atoms (in parts per million). For these measurements, reference materials MgO and Al_2O_3 were employed. The samples of LiF and the reference materials (MgO and Al_2O_3) were individually placed in small polyethylene vials. Iron wires were attached to the outside of each vial to monitor the flux. The activation of ^{56}Fe results in the production of ^{56}Mn which has a half-life of 2.582 hours and decays by beta emission accompanied predominantly by a 0.846 MeV gamma ray. After irradiation, energy spectra were made of the samples, references, and flux monitors on the pulse height analyzer. Integration of the photoelectric peaks was used to determine the number of gamma counts.

The expression used in determining the impurity concentrations in ppm, which is developed from Eq. (A.3), is

$$\frac{N_{os}}{N'_{o}} \times \frac{N'_{ofe}}{N_{osfe}} \times 10^6 = \text{ppm} , \qquad (A.4)$$

where

$N_{os} = Ne^{+\lambda\tau}/\text{mass of crystal},$

$N'_{o} = Ne^{+\lambda\tau}/(\text{mass of reference}) \times (\% \text{ of isotope}),$

N'_{ofe} or $N_{osfe} = Ne^{+\lambda\tau}/\text{mass of wire}.$

It can be seen that the terms τ, ϕ_o, σ, and $(1-e^{-\lambda t})$ in Eq. (A.3) are not considered when determining ppm because they cancel out.

The following results were received from the quantitative neutron activation analysis;

1)   Harshaw samples (1975 crystals) contained aluminum at a concentration of 2.5 $\pm$ 0.8,

2)   Optovac samples contained aluminum and magnesium at concentrations of 3.5 $\pm$ 0.8 ppm and 32.0 $\pm$ 8.0 ppm, respectively,

3)   Harshaw samples (1972 crystals) contained aluminum and magnesium at concentrations of 22.5 $\pm$ 1.0 ppm and 51.0 $\pm$ 11.0 ppm, respectively.

Appendix B

Determination of the Spectral Distribution of the Xenon Lamp and Normalization
of Photocurrents

The spectral distribution of the xenon lamp must be determined at the sample
position so the photoconductivity spectra can be normalized to a constant photon
flux. The experimental setup used in determining the spectral distribution of the
lamp is shown in Fig. 29. A Tungsten-Iodide Standard Lamp (Model L-101) and Power
Supply (Model P-101) was used to determine the sensitivity of the Bausch and
Lomb Monochromator and the Jarrell-Ash Photomultiplier (PM) Tube (Type 1P28,
with a S5 response). The photocathode of the PM tube was at the same distance
from the exit slit of the monochromator as the photoconductivity sample, and the
tube was biased at -750 volts with a Fluke High Voltage Power Supply (Model
415B). A Keithley Picoammeter (Model 410A) measured the PM output, and plotted
it (PM output) versus wavelength on a Hewlett-Packard 7004A-116 X-Y Plotter.
This method was used to determine the output of both the xenon lamp and the
standard lamp.

The sensitivity of the monochromator-PM tube system (in milliamp/µwatt),
was determined by measuring its response to the standard lamp. The power-
spectral distribution for the standard lamp is given by the following
expression,

$$I_{40} = \frac{\alpha}{\lambda^5 (e^{\beta/\lambda} - 1)} , \tag{B.1}$$

where

$\alpha = 6.768 \times 10^{-8}$ µW·cm^3/10 $\overset{\circ}{A}$,

$\beta = 4.593 \times 10^{-4}$ cm,

$\lambda =$ wavelength in cm,

$I_{40} =$ spectral radiance in µW/cm^2·10 $\overset{\circ}{A}$ at 40 cm from the monochromator
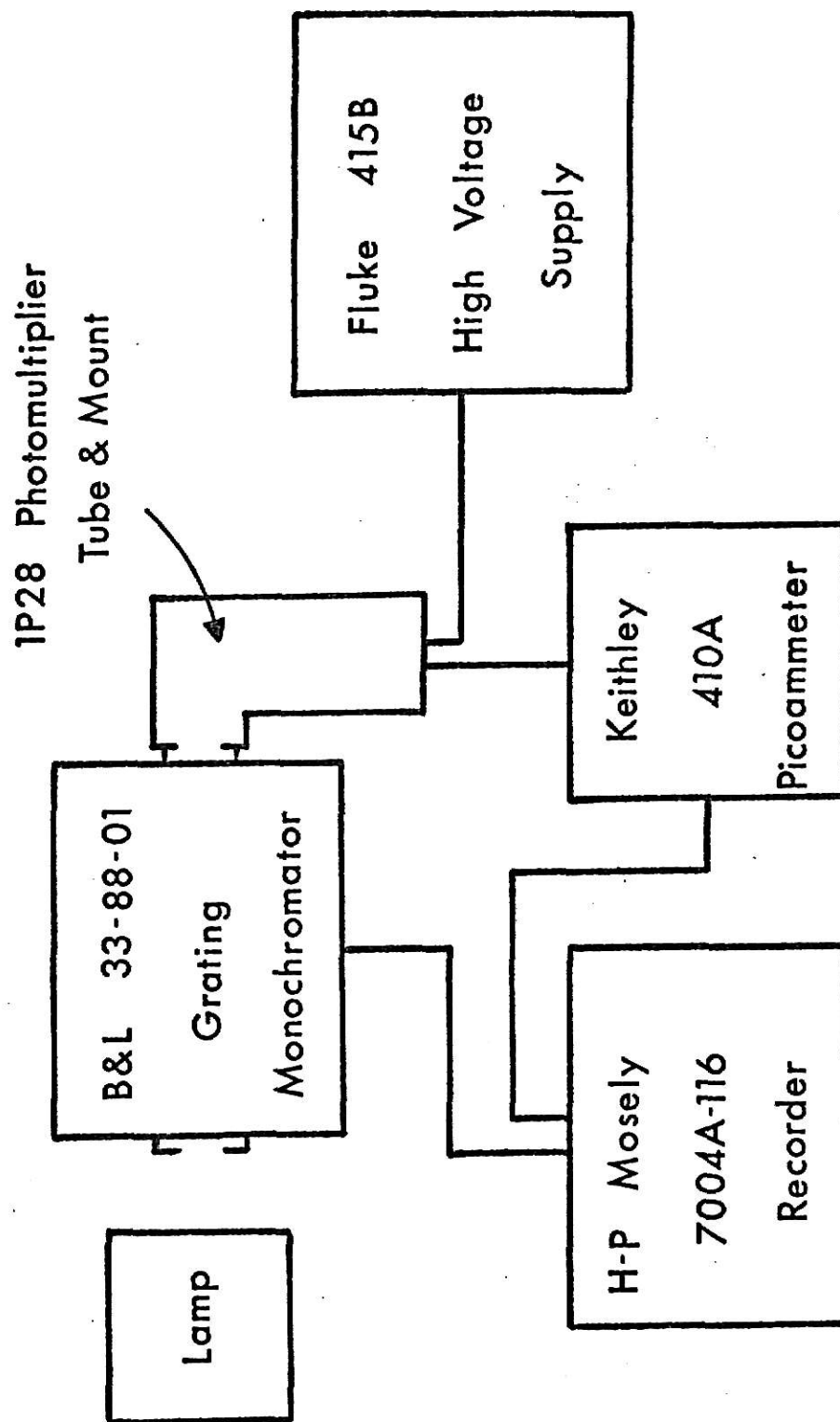
entrance slit.

FIGURE 29: Experimental arrangement for the determination of the radiative power of the Xenon Lamp. Lamp denotes either the Tungsten-Iodide Standard Lamp or the 150 watt Xenon Lamp.

The standard lamp was not 40 cm from the entrance slit of the monochromator, but at 15.6 cm; so a correction to the spectral radiance was made by use of the inverse square law[31],

$$\frac{I_{15.6}}{I_{40}} = \frac{(40)^2}{(15.6)^2} \tag{B.2}$$

where $I_{15.6}$ is the spectral radiance in $\mu W/cm^2 \cdot 10$ Å at 15.6 cm. In order to determine the sensitivity of the monochromator-PM tube, the observed current output of the PM tube for the standard lamp at a specific wavelength is divided by $I_{15.6}$, calculated for the same wavelength, the area of illumination of the photocathode and the bandpass of the monochromator.

To determine the power output of the xenon lamp, the observed current output of the PM tube, at a specific wavelength, is divided by the sensitivity of the monochromator-PM tube at the same wavelength. The power output of the xenon lamp incident at the sample location as a function of wavelength is shown on Fig. 30.

The determination of the photon flux of a lamp is formulated in the following manner. By definition,

$$\text{Intensity} = \text{Average Power/Area} , \tag{B.3}$$

and

$$\text{Intensity} = (\text{Number of photons})(\text{unit area})^{-1}(\text{unit time})^{-1}$$

$$\times (\text{Energy of a single photon}) \tag{B.4}$$

Combining Eqs. (B.3) and (B.4) and solving for the photon flux, N, gives

$$N = I/E = (P/E) \times (1/A) \tag{B.5}$$

where

I = intensity of the light,

E = energy of a single photon in eV,

A = area of illumination in cm^2,
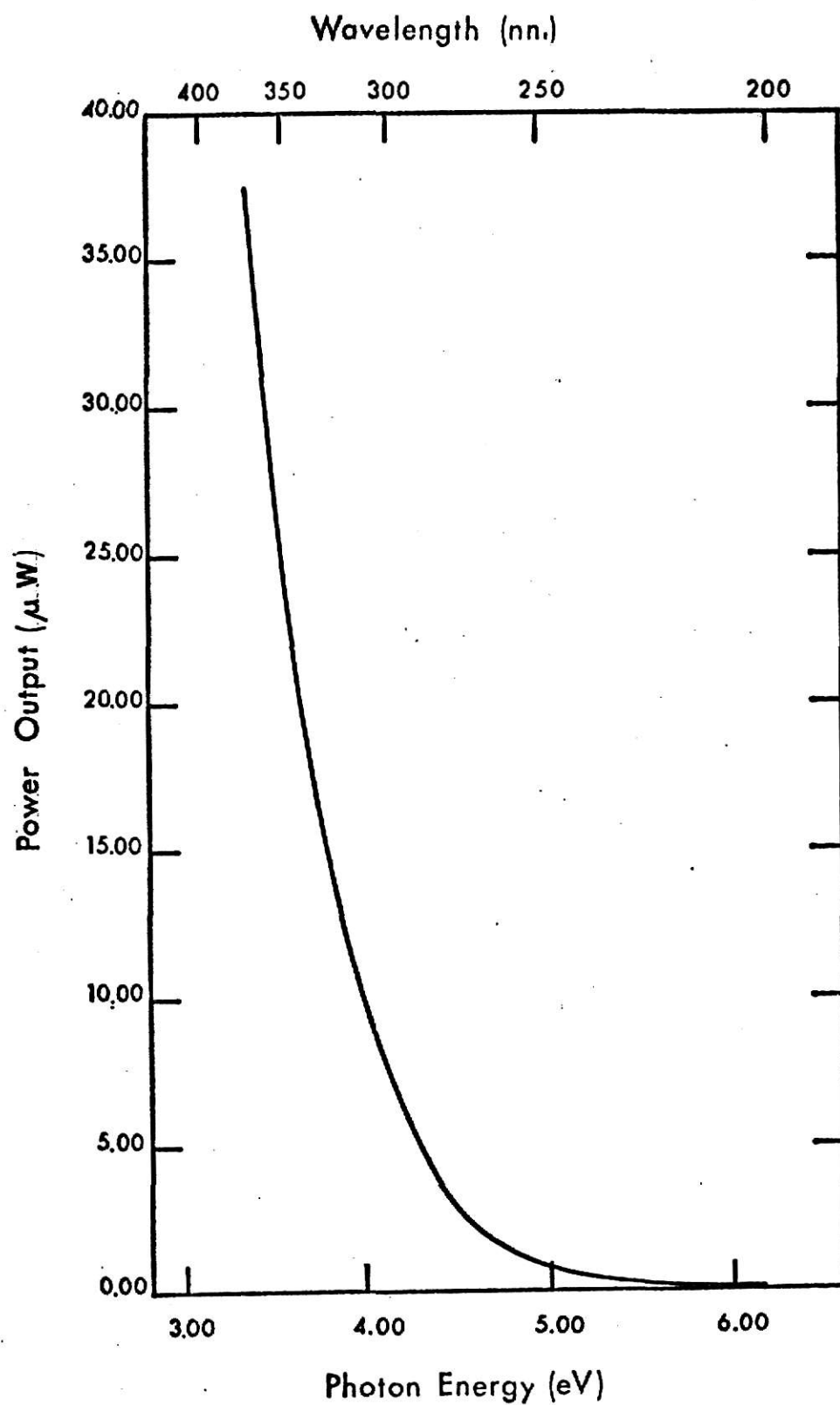
P = power in watts.

FIGURE 30: Power output of the Xenon Lamp incident on the front surface of the sample

Using Eq. (B.5), the photon flux can be determined for a specific wavelength and the corresponding photocurrent. The photon flux is determined at 370 nm using the following values:

P = power of the incident light at 370 nm = 37.5 µW,

A = area of illumination = 0.126 cm^2,

E = energy of a photon at 370 nm = 3.35 eV.

The photocurrent is then normalized, by a proportion, to a photon flux of 5.55×10^{14} photons/cm^2·sec at 370 nm.

A STUDY OF THE OPTICAL ABSORPTION AND PHOTOCONDUCTIVITY
OF GAMMA-IRRADIATED LiF

by

MILTON HENRY RICHTER

B.S., Valparaiso University, 1974

AN ABSTRACT OF A MASTER'S THESIS

submitted in partial fulfillment of the
requirements for the degree

MASTER OF SCIENCE

Department of Nuclear Engineering

Kansas State University

Manhattan, Kansas

1976

Abstract

The optical absorption and photoconductivity of gamma-irradiated LiF was studied to determine the cause of an unresolved absorption band, labeled the Y-center, on the low energy side (4.4 eV) of the F-center absorption band. LiF having different impurity concentrations was used to identify the positive ion impurity believed to be causing the Y-center. The Y-center absorption was studied with polarized light ([011] and [0$\bar{1}$1] directions) and found to exhibit dichroic behavior. The Y-center absorption band can also be optically bleached. Photoconductivity from the Y-center was not observed in unirradiated LiF, but a definite Y-center photocurrent was observed for gamma-irradiated LiF. The photocurrent is discussed in terms of the fundamental processes in a photoconductor and the characteristic relations of photoconductivity. From the results of the optical absorption and photoconductivity measurements, an expansion of a previously proposed model for the Y-center is made.